

Quantum Backreaction in Effective Brans-Dicke Bianchi I Cosmology

Hector Hernandez-Hernandez^{1,2,*} and Gustavo Sanchez-Herrera^{3,†}

¹Universidad Autonoma de Chihuahua, Facultad de Ingenieria,
Nuevo Campus Universitario, Chihuahua 31125, Mexico

²Universidad Autonoma Metropolitana- Cuajimalpa,
Departamento de Matematicas Aplicadas y Sistemas, Vasco de Quiroga 4871, 05348, Mexico

³Universidad Autonoma Metropolitana- Iztapalapa,
Departamento de Fisica, Ciudad de Mexico, 09340, Mexico

We investigate the effective quantum evolution of the Bianchi type I cosmological model within the Brans-Dicke framework using an effective Hamiltonian approach that includes expectation values, quantum dispersions and cross-correlation terms between different degrees of freedom. For the case $\omega < -3/2$, where energy conditions are violated and bouncing solutions exist classically, we demonstrate that quantum backreaction effects significantly smooth the bounce of directional scale factors, with the bounce occurring at scales set by the quantum state width. For the conformally invariant case $\omega = -3/2$, quantum corrections cause scale factors to enter accelerated expansion phases more rapidly than in the classical limit. Most significantly, we show that cross-correlation terms between canonical variables are essential for obtaining physically consistent effective dynamics: neglecting these terms leads to spurious divergences and unphysical behavior. When correlations are included, small-amplitude oscillations appear shortly after the bounce, rapidly damping to classical trajectories. We interpret these oscillations as quantum remnant effects encoding information about correlations between gravitational and scalar field degrees of freedom. Our results demonstrate that cross-correlations carry crucial quantum information that substantially influences cosmological dynamics, with implications for quantum gravity phenomenology near singularities. We compare our findings with existing loop quantum cosmology results.

I. INTRODUCTION

General Relativity (GR), formulated by Einstein in 1915 [1], has achieved remarkable empirical success over the past century. Its predictions, from the anomalous precession of Mercury's perihelion [2] and gravitational light deflection [3] to the existence of black holes [4] and gravitational waves [2, 5], have been repeatedly confirmed with increasing precision. Nevertheless, several fundamental challenges indicate that GR cannot be the complete description of gravitational phenomena.

Most prominently, GR predicts its own breakdown at cosmological singularities, both the Big Bang and black hole interiors, where spacetime curvature diverges [6, 7]. These singularities signal the need for a quantum theory of gravity. Additionally, observations of galactic rotation curves [8], large-scale structure formation [9], and the accelerated cosmic expansion [10, 11] require either the introduction of dark matter and dark energy, or modifications to gravitational dynamics itself. These puzzles have motivated extensive investigations of both quantum gravity and modified gravity theories.

Among the earliest and most influential generalizations of GR is the Brans-Dicke (BD) theory [12], developed in 1961 to incorporate Mach's principle into gravitational physics. In BD theory, Newton's gravitational constant G is promoted to a dynamical scalar field ϕ , with $G \propto \phi^{-1}$. The theory contains a dimensionless parameter ω

that governs the strength of the coupling between the scalar field and gravity. Solar system tests constrain $\omega > 40,000$ for standard BD theory [13, 14], although these constraints can be evaded in modified versions [15].

Despite these tight observational bounds on positive ω , the case of negative coupling constants, particularly $\omega < -3/2$, presents unique theoretical interest. In this regime, energy conditions are violated [16], potentially allowing for nonsingular bouncing cosmologies without exotic matter [17], connections to string theory effective actions [18, 19], accelerated expansion mechanisms [20], and wormhole solutions [21].

The special case $\omega = -3/2$ is particular: the theory becomes conformally invariant [22, 23] and dynamically equivalent to Palatini $f(R)$ gravity [24]. This equivalence connects BD theory to a broader class of modified gravity theories with potential observational signatures [25, 26].

Recent cosmological tensions, the Hubble tension [27] and S_8 tension [28], for instance, have renewed interest in BD theory as a possible resolution mechanism [25, 26, 29, 30]. Whether these applications require $\omega < 0$ remains an active area of investigation.

A fundamental hypothesis for quantum gravity is the resolution of classical singularities through quantum effects. Loop Quantum Cosmology (LQC), the cosmological sector of Loop Quantum Gravity (LQG) [31, 32], has demonstrated singularity replacement by quantum bounces in the homogeneous, isotropic (FLRW) model [33, 34]. The mechanism relies on quantum geometry effects becoming dominant near the Planck scale, generating an effective repulsive force that prevents collapse to infinite density.

* hernandez@uach.mx

† cbi2233805002@xanum.uam.mx

Extensions to anisotropic models, particularly Bianchi cosmologies, are crucial for several reasons. Some of the most important are 1) the Belinskii-Khalatnikov-Lifshitz (BKL) conjecture [35, 36] proposes that generic spacetimes near singularities exhibit chaotic Bianchi-type dynamics, making anisotropic models phenomenologically essential, 2) anisotropies may leave observational imprints in the cosmic microwave background [37], 3) technical complexities of anisotropic models test the robustness of quantum gravity approaches. Loop quantum Bianchi I models have been studied in GR [38, 39], demonstrating singularity resolution with bounded curvature invariants. However, full quantum evolution equations remain challenging to solve analytically for systems with reduced symmetry.

For complex quantum systems where the full Schrödinger or Wheeler-DeWitt equation is intractable, effective quantum theories provide a powerful alternative [40, 41]. Rather than solving for the complete wavefunction Ψ , one works directly with expectation values $\langle \hat{O} \rangle$, quantum dispersions $\Delta(\hat{O}^2) = \langle (\hat{O} - \langle \hat{O} \rangle)^2 \rangle$, and correlations between observables. The effective Hamiltonian approach, developed systematically in [40–42], expands the expectation value of the quantum Hamiltonian in powers of quantum moments:

$$H_{\text{eff}} = \langle \hat{H} \rangle = H_{\text{cl}}[\langle \hat{q} \rangle, \langle \hat{p} \rangle] + \sum_{n=2}^{\infty} H^{(n)}[\Delta(q^a p^b)], \quad (1)$$

where $H^{(n)}$ contains contributions from n -th order moments. Truncating at a given order yields a finite-dimensional extended phase space including expectation values up to that order in moments.

This approach has successfully reproduced known results in isotropic quantum cosmology [43] while enabling studies of more complex scenarios: anisotropic Bianchi models [44], inhomogeneous cosmologies [45], black hole interiors [46] and general quantum systems [47, 48].

A critical aspect often overlooked in effective approaches is the role of cross-correlation terms, quantum moments coupling different degrees of freedom, such as $\Delta(q_i p_j)$ with $i \neq j$ or $\Delta(q_i \phi)$ between gravitational and matter variables. Recent work has demonstrated that correlations can substantially modify the dynamics [49, 50]: neglecting correlations may miss crucial quantum effects because they encode nonlocal quantum information and, in some systems, correlations prevent unphysical behavior. Despite their importance, systematic studies of cross-correlations in quantum cosmology remain limited, particularly for modified gravity theories.

In this paper, we investigate the effective quantum dynamics of the Bianchi I cosmological model within Brans-Dicke theory, with particular focus on studying how do quantum corrections modify classical bouncing solutions (quantum backreaction); analysing what is the quantitative impact of cross-correlations on dynamics and whether they are essential for consistency; investigating the coupling parameter dependence and the physical in-

terpretation of our findings such as the nature of post-bounce oscillations and how do quantum remnants manifest.

Organization. This paper is structured as follows. In section II we review the Hamiltonian formulation of Brans-Dicke theory for Bianchi I spacetime and present classical dynamics for both coupling constant regimes (all technical details in the Appendix A). In section III we develop the effective quantum formalism and derive the second-order effective Hamiltonian, with a discussion of the truncation validity. In section IV we present numerical results, emphasizing the crucial role of cross-correlations. In section V we compare our findings with previous work and discusses physical interpretation. Finally, in section VI we summarize results and outline future directions. Appendix A contains ADM formulation details, Appendix B gives complete equations of motion.

II. CLASSICAL BRANS-DICKE BIANCHI I COSMOLOGY

In this section, we establish the classical framework for our quantum effective analysis. We begin with the Hamiltonian formulation of Brans-Dicke theory specialized to Bianchi type I spacetime (Sec. II A), then analyze the classical dynamics for two physically distinct cases: generic negative coupling $\omega < -3/2$ (Sec. II B) and the conformally invariant case $\omega = -3/2$ (Sec. II C).

A. Hamiltonian Formulation in Ashtekar Variables

1. Bianchi I Geometry and Canonical Variables

The Bianchi type I model describes spatially homogeneous, anisotropic, and spatially flat cosmologies. The metric takes the diagonal form

$$ds^2 = -N^2 dt^2 + a_1^2(t) dx_1^2 + a_2^2(t) dx_2^2 + a_3^2(t) dx_3^2, \quad (2)$$

where $N(t)$ is the lapse function and $a_i(t)$ are directional scale factors. Spatial homogeneity allows reduction to a finite-dimensional phase space after introducing a fiducial cell \mathcal{V}_0 with volume $V_0 = L_1 L_2 L_3$ [38].

We employ Ashtekar-Barbero variables [51, 52], which recast gravitational phase space in terms of an $\mathfrak{su}(2)$ -valued connection A_a^i and its conjugate densitized triad E_i^a . For Bianchi I, symmetry reduction yields [38]

$$A_a^i = c_i(L_i)^{-1} \dot{e}_a^i, \quad E_i^a = p_i L_i V_0^{-1} \sqrt{\dot{q}} \dot{e}_a^i, \quad (3)$$

where \dot{e}_a^i is a fiducial triad with determinant \dot{q} , and (c_i, p_i) are time-dependent canonical variables satisfying

$$\{c_i, p_j\} = 8\pi G \gamma \delta_{ij}, \quad (4)$$

with γ the Barbero-Immirzi parameter [53].

The directional scale factors are related to p_i by (choosing positive orientation and $L_i = 1$)

$$a_1 = \sqrt{\frac{p_2 p_3}{p_1}}, \quad a_2 = \sqrt{\frac{p_1 p_3}{p_2}}, \quad a_3 = \sqrt{\frac{p_1 p_2}{p_3}}. \quad (5)$$

The mean scale factor is $a = (a_1 a_2 a_3)^{1/3} = (p_1 p_2 p_3)^{1/6} \equiv p^{1/6}$.

Physical observables include directional Hubble parameters

$$H_i \equiv \frac{\dot{a}_i}{a_i} = \frac{1}{2} \left(\sum_{j \neq i} \frac{\dot{p}_j}{p_j} - \frac{\dot{p}_i}{p_i} \right), \quad (6)$$

and the shear scalar, measuring anisotropy:

$$\sigma^2 = \frac{1}{3} \sum_{i < j} (H_i - H_j)^2. \quad (7)$$

2. Brans-Dicke Action and Hamiltonian Constraint

The Brans-Dicke action is [12, 15]

$$S_{\text{BD}} = \frac{1}{16\pi} \int d^4x \sqrt{-g} \left[\phi R - \frac{\omega}{\phi} g^{\mu\nu} \partial_\mu \phi \partial_\nu \phi \right], \quad (8)$$

where ϕ is the Brans-Dicke scalar (related to the gravitational constant by $G_{\text{eff}} = 1/\phi$) and ω is the dimensionless coupling constant. We work in units where $16\pi G = 1$ and set $\gamma = 1$ for simplicity.

Following the procedure detailed in Appendix A, the Hamiltonian constraint for Bianchi I in Ashtekar variables becomes [54, 55]:

a. *Case I: $\omega \neq -3/2$ (Generic Coupling).* For $\omega < -3/2$, the Hamiltonian constraint is

$$\mathcal{H}_{\text{BD}} = -\frac{N}{\gamma^2 \phi \sqrt{p}} (S - \zeta T^2) \approx 0, \quad (9)$$

where we defined

$$S \equiv c_1 c_2 p_1 p_2 + c_1 c_3 p_1 p_3 + c_2 c_3 p_2 p_3, \quad (10a)$$

$$T \equiv \sum_{i=1}^3 c_i p_i + \gamma^{-1} \phi p_\phi, \quad (10b)$$

$$\zeta \equiv \frac{1}{3 + 2\omega}, \quad (10c)$$

and (ϕ, p_ϕ) are canonical variables for the scalar field with $\{\phi, p_\phi\} = 1$.

b. *Case II: $\omega = -3/2$ (Conformal Invariance).* For $\omega = -3/2$, the term proportional to T^2 diverges and the theory becomes conformally invariant [22, 23], requiring a modified constraint structure. The Hamiltonian constraint becomes in this case

$$\mathcal{H}_{\text{BD}}^c = -\frac{N}{\gamma^2 \phi \sqrt{p}} S + \frac{\lambda}{\gamma} \left(\sum_{i=1}^3 c_i p_i - \phi p_\phi \right) \approx 0, \quad (11)$$

where λ is a Lagrange multiplier enforcing an additional constraint

$$\mathcal{C}_S = \sum_{i=1}^3 c_i p_i - \phi p_\phi \approx 0. \quad (12)$$

The constraint (12) arises from conformal invariance and does not contain new physical information—it merely relates momenta. The multiplier λ is determined by consistency of constraints but does not affect physical predictions [22].

3. Physical Quantities

The energy density, computed from the Hamiltonian constraint, is

$$\rho = \frac{1}{N \sqrt{p}} \mathcal{H}_{\text{BD}} = \begin{cases} -\frac{1}{\gamma^2 \phi p} (S - \zeta T^2), & \omega \neq -3/2 \\ -\frac{1}{\gamma^2 \phi p} S, & \omega = -3/2 \end{cases} \quad (13)$$

For the effective quantum analysis, we will need ρ expressed in terms of expectation values. In the quantum case, quantum dispersions and correlations will contribute additional terms.

B. Classical Dynamics: Case $\omega < -3/2$

1. Equations of Motion

Hamilton's equations $\dot{f} = \{f, \mathcal{H}_{\text{BD}}\}$ with the constraint (9) yield (setting $N = \gamma = 1$):

$$\begin{aligned} \dot{c}_1 &= \frac{1}{\phi \sqrt{p}} \left[-c_1 (c_2 p_2 + c_3 p_3 - 2\zeta T) + \frac{S - \zeta T^2}{2p_1} \right], \\ \dot{c}_2 &= \frac{1}{\phi \sqrt{p}} \left[-c_2 (c_1 p_1 + c_3 p_3 - 2\zeta T) + \frac{S - \zeta T^2}{2p_2} \right], \\ \dot{c}_3 &= \frac{1}{\phi \sqrt{p}} \left[-c_3 (c_1 p_1 + c_2 p_2 - 2\zeta T) + \frac{S - \zeta T^2}{2p_3} \right], \\ \dot{p}_1 &= \frac{\sqrt{p}}{\phi} \left(c_2 p_3 + c_3 p_2 - \frac{2p_1 \zeta T}{p} \right), \\ \dot{p}_2 &= \frac{\sqrt{p}}{\phi} \left(c_1 p_3 + c_3 p_1 - \frac{2p_2 \zeta T}{p} \right), \\ \dot{p}_3 &= \frac{\sqrt{p}}{\phi} \left(c_1 p_2 + c_2 p_1 - \frac{2p_3 \zeta T}{p} \right), \\ \dot{\phi} &= \frac{2\zeta}{\sqrt{p}} T, \\ \dot{p}_\phi &= -\frac{1}{\phi^2 \sqrt{p}} (S + 2\gamma \zeta \phi p_\phi T - \zeta T^2). \end{aligned} \quad (14)$$

We analyze this system numerically.

2. Bouncing Solutions and Initial Conditions

For $\omega < -3/2$, the parameter $\zeta < 0$, and the term $-\zeta T^2 > 0$ in the Hamiltonian constraint (9) can dominate near small volumes, generating an effective repulsive

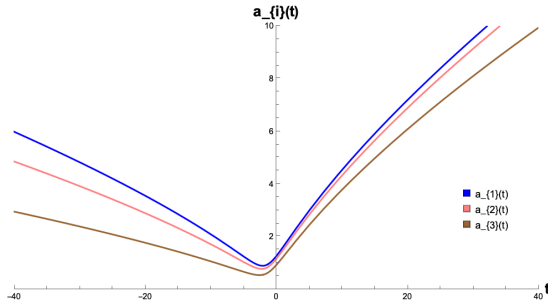


FIG. 1. Classical evolution of directional scale factors $a_i(t)$ for Brans-Dicke Bianchi I with $\omega = -5$. All three directions exhibit smooth bounces, with anisotropic structure evident in different bounce amplitudes. Initial conditions are given in Eq. (15).

force. This leads to bouncing solutions where scale factors reach a minimum (the bounce) and then re-expand [16, 17].

To explore this regime, we choose $\omega = -5$ (giving $\zeta = -1/7$) and initial conditions

$$\begin{aligned} c_1(0) &= 1.2, & p_1(0) &= 1.1, \\ c_2(0) &= 1.3, & p_2(0) &= 1.2, \\ c_3(0) &= 1.4, & p_3(0) &= 1.5, \\ \phi(0) &= 10, & p_\phi(0) &= 1. \end{aligned} \quad (15)$$

These values are chosen to place the system in a contracting phase approaching a bounce. While not derived from specific physical scenarios, they allow clear demonstration of bouncing dynamics. In realistic cosmological applications, initial conditions would be constrained by late-time observations propagated backwards.

3. Numerical Results

Figure 1 shows the evolution of scale factors $a_i(t)$ obtained by numerical integration of Eqs. (14). All three directional scale factors exhibit smooth bounces near $t \approx 0$, with minimum values $a_i^{\min} \sim (0.8-1.1)$ depending on direction. The anisotropy is evident: different directions have different bounce times and minimum scales.

Figure 2 displays the corresponding directional Hubble parameters $H_i(t)$ computed from Eq. (6). Each H_i transitions from negative (contraction) through zero (bounce) to positive (expansion). The asymptotic behavior is $H_i \rightarrow 0$ as $t \rightarrow \pm\infty$, indicating approach to Minkowski space at early and late times in this configuration.

The energy density $\rho(t)$ (Fig. 3) remains finite throughout evolution, reaching a maximum $\rho_{\max} \approx 7.3$ (in Planck units with our normalization) at the bounce. This finiteness is a key feature: despite the classical bounce, no energy singularity occurs.

The shear $\sigma(t)$ in Figure 4 measures anisotropy. It peaks near the bounce and decays as the universe expands, indicating isotropization at late times. This be-

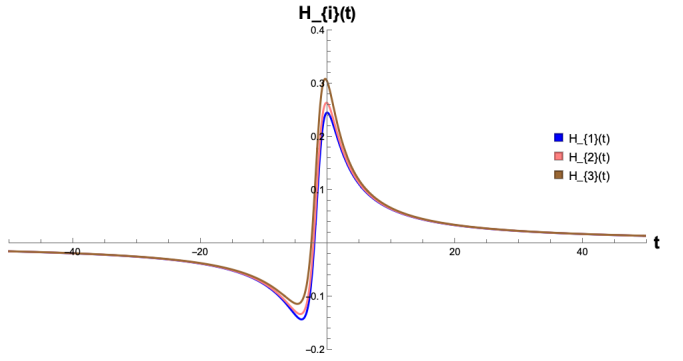


FIG. 2. Directional Hubble parameters $H_i(t)$ for the evolution in Fig. 1. Negative values indicate contraction; positive values indicate expansion. Zero crossings mark the bounce points, which occur at slightly different times for different directions due to anisotropy.

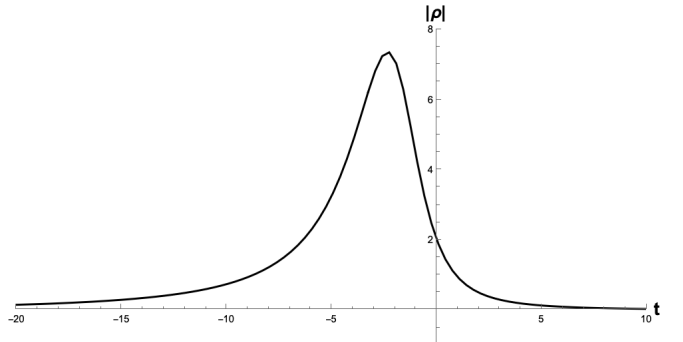


FIG. 3. Energy density $\rho(t)$ for $\omega = -5$ case, computed from Eq. (13). The density remains finite at the bounce, reaching $\rho_{\max} \approx 7.3$. This demonstrates classical energy singularity avoidance in BD theory with $\omega < -3/2$.

havior is consistent with general expectations for Bianchi I models without matter sources that preferentially drive anisotropy.

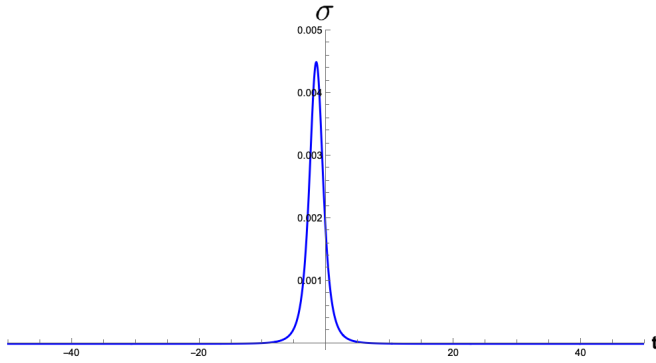


FIG. 4. Shear $\sigma(t)$ quantifying anisotropy for $\omega = -5$. The shear peaks near the bounce where directional expansion rates differ most significantly, then decays as the universe isotropizes during expansion.

C. Classical Dynamics: Case $\omega = -3/2$

1. Equations of Motion with Lagrange Multiplier

For the conformally invariant case, Hamilton's equations derived from (11) yield (setting $N = \gamma = 1$):

$$\begin{aligned} \dot{c}_1 &= -\frac{1}{2\phi\sqrt{p}} \left(c_1 c_2 p_2 + c_1 c_3 p_3 - \frac{c_2 c_3 p_2 p_3}{p_1} \right) + \lambda c_1, \\ \dot{c}_2 &= -\frac{1}{2\phi\sqrt{p}} \left(c_1 c_2 p_1 + c_2 c_3 p_3 - \frac{c_1 c_3 p_1 p_3}{p_2} \right) + \lambda c_2, \\ \dot{c}_3 &= -\frac{1}{2\phi\sqrt{p}} \left(c_1 c_3 p_1 + c_2 c_3 p_2 - \frac{c_1 c_2 p_1 p_2}{p_3} \right) + \lambda c_3, \\ \dot{p}_1 &= \frac{\sqrt{p}}{\phi} (c_3 p_2 + c_2 p_3) - \lambda p_1, \\ \dot{p}_2 &= \frac{\sqrt{p}}{\phi} (c_3 p_1 + c_1 p_3) - \lambda p_2, \\ \dot{p}_3 &= \frac{\sqrt{p}}{\phi} (c_2 p_1 + c_1 p_2) - \lambda p_3, \\ \dot{\phi} &= -\lambda\phi, \\ \dot{p}\phi &= -\frac{S}{\phi^2\sqrt{p}} + \lambda p\phi. \end{aligned} \quad (16)$$

The Lagrange multiplier λ enters linearly in each equation. It is not a dynamical variable but a constraint multiplier whose value must be determined consistently. It affects the time parametrization but not physical observables expressible as ratios of evolving quantities.

To understand its role, consider the evolution of ϕ :

$$\phi(t) = \phi(0)e^{-\lambda t}. \quad (17)$$

Different values of λ correspond to different time slicings of the same physical spacetime [22]. Observables like the scale factors at a given value of ϕ are independent of λ .

For numerical studies, we choose $\lambda = 1$ as a reference value. We verify that physical conclusions are λ -independent by comparing results for different values (see Sec. IV B).

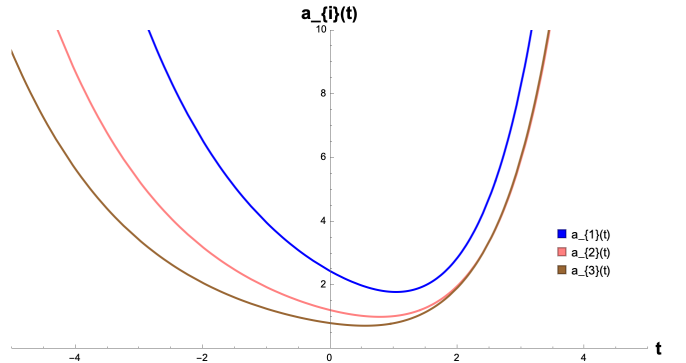


FIG. 5. Classical evolution of scale factors $a_i(t)$ for the conformally invariant case $\omega = -3/2$ with $\lambda = 1$. Smooth bounces occur, structurally similar to the $\omega = -5$ case but with different bounce scales and asymptotic behavior. Initial conditions from Eq. (18).

2. De Sitter Asymptotics

An interesting feature of the $\omega = -3/2$ case is its asymptotic de Sitter behavior [20]. From Eq. (16), one can show that as $t \rightarrow \pm\infty$, each H_i approaches a constant value $H_i \rightarrow H_\infty$, implying exponential expansion (or contraction) $a_i \sim e^{H_\infty t}$.

This is related to conformal invariance: the theory admits solutions asymptotically approaching de Sitter space, which is conformally flat. Such behavior has been explored as a mechanism for early universe inflation [20] and late-time acceleration [56].

3. Numerical Results

We evolve Eqs. (16) with initial conditions

$$\begin{aligned} c_1(0) &= 1.1, & p_1(0) &= 1.0, \\ c_2(0) &= 1.2, & p_2(0) &= 2.0, \\ c_3(0) &= 1.3, & p_3(0) &= 3.0, \\ \phi(0) &= 10, & p_\phi(0) &= 1.0, \end{aligned} \quad (18)$$

and $\lambda = 1$.

Figure 5 shows the scale factors evolution. As in the $\omega = -5$ case, smooth bounces occur, but now with different quantitative features due to the modified dynamics.

Figure 6 displays the Hubble parameters. Instead of asymptotically approaching zero, each H_i approaches a constant value $H_{+\infty} \approx 1.1$, and $H_{-\infty} \approx -0.5$ (determined by λ and initial conditions). This constant Hubble parameter signals de Sitter expansion at late times and de Sitter contraction at early times, with the bounce interpolating between these phases.

Figure 7 demonstrates λ -independence of physical predictions, which can be seen in a plot of $a_i(t)(\lambda)$. While the absolute time coordinate of the bounce shifts with

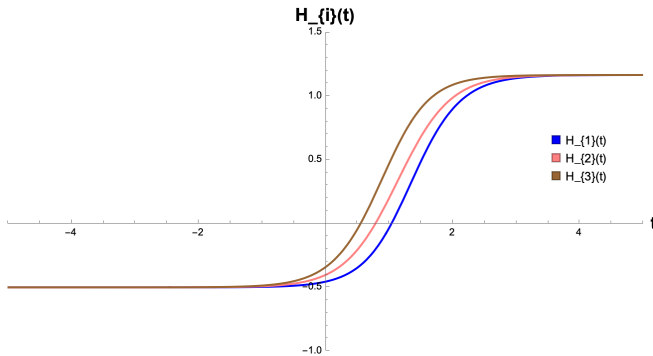


FIG. 6. Directional Hubble parameters for $\omega = -3/2$. Unlike the $\omega = -5$ case, here H_i asymptotes to constant values $H_{+\infty} \approx 1.1$, and $H_{-\infty} \approx -0.5$ rather than zero, indicating asymptotic de Sitter contraction (past) and expansion (future). This is a signature of conformal invariance.

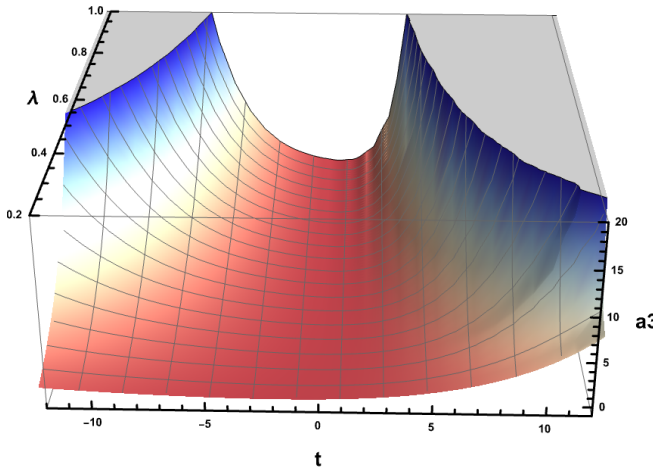


FIG. 7. Dependence of the scale factor $a_3(t)$ on the Lagrange multiplier λ for $\omega = -3/2$. Different values of λ shift the bounce time but preserve physical structure. This demonstrates that λ affects time parametrization only, not physical predictions.

λ , the bounce structure and scale factor values at corresponding physical times (e.g., at fixed ϕ) remain unchanged.

Energy density and shear (Figs. 8 and 9) exhibit qualitatively similar behavior to the $\omega = -5$ case: finite ρ at the bounce and shear peaking near the bounce then decaying.

D. Summary of Classical Dynamics

Both cases $\omega = -5$ and $\omega = -3/2$ exhibit:

- Smooth bouncing solutions with finite energy density;
- Anisotropic evolution (different bounce times and amplitudes for different directions);

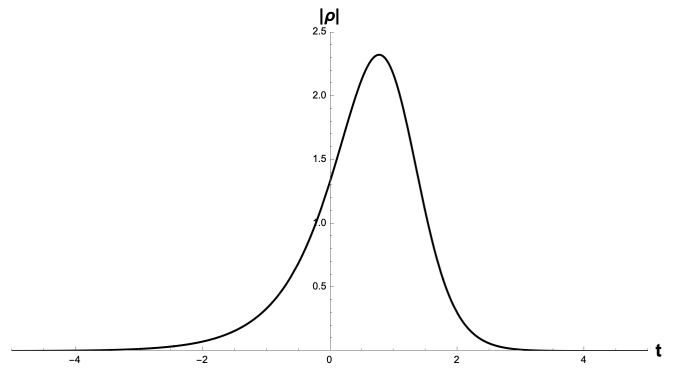


FIG. 8. Energy density for $\omega = -3/2$, remaining finite at the bounce with $\rho_{\max} \approx 2.3$.

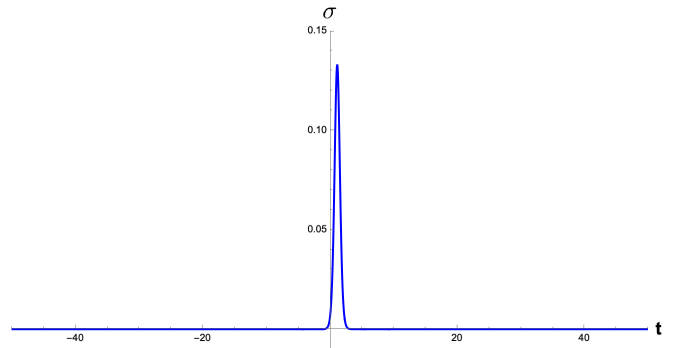


FIG. 9. Shear evolution for $\omega = -3/2$, showing peak near bounce and subsequent decay.

- Classical singularity avoidance via the BD scalar field mechanism.

Key differences:

- Asymptotic behavior: $H_i \rightarrow 0$ for $\omega = -5$; $H_i \rightarrow H_{\infty} \neq 0$ for $\omega = -3/2$;
- Constraint structure: Single Hamiltonian constraint vs. Hamiltonian plus conformal constraint
- Time parametrization: Standard for $\omega < -3/2$; λ -dependent for $\omega = -3/2$.

In the following sections, we investigate how quantum effects modify these classical bouncing scenarios.

III. EFFECTIVE QUANTUM DYNAMICS

We now develop the effective quantum formalism for the Brans-Dicke Bianchi I model. After reviewing the general effective approach (Sec. III A), we construct the second-order effective Hamiltonian (Sec. III B) and discuss its regime of validity (Sec. III C).

A. General Effective Formalism

We provide now an effective quantum analysis of the model at hand by working directly with expectation values and quantum moments.

1. Quantum Moments and Extended Phase Space

Consider a quantum system with canonical variables (\hat{q}_i, \hat{p}_i) satisfying $[\hat{q}_i, \hat{p}_j] = i\hbar\delta_{ij}$. We define expectation values

$$\langle \hat{q}_i \rangle \equiv q_i, \quad \langle \hat{p}_i \rangle \equiv p_i, \quad (19)$$

and quantum moments (using Weyl ordering for symmetrization):

$$\Delta(q_i^a p_j^b) \equiv \langle (\hat{q}_i - q_i)^a (\hat{p}_j - p_j)^b \rangle_{\text{Weyl}}. \quad (20)$$

With $a + b = 2$. The correlations and moments:

$$\Delta(q_i^2) = \langle (\hat{q}_i - q_i)^2 \rangle = (\Delta q_i)^2, \quad (21a)$$

$$\Delta(p_i^2) = \langle (\hat{p}_i - p_i)^2 \rangle = (\Delta p_i)^2, \quad (21b)$$

$$\Delta(q_i p_i) = \frac{1}{2} \langle \{ \hat{q}_i - q_i, \hat{p}_i - p_i \} \rangle. \quad (21c)$$

For $i \neq j$, $\Delta(q_i p_j)$, $\Delta(q_i q_j)$, and $\Delta(p_i p_j)$ are the cross-correlations between different degrees of freedom.

The quantum moments satisfy Heisenberg uncertainty relations. For a single degree of freedom:

$$\Delta(q^2) \Delta(p^2) - \Delta(qp)^2 \geq \frac{\hbar^2}{4}. \quad (22)$$

For multiple degrees of freedom, more complex uncertainty relations exist, involving cross-correlations [41].

2. Effective Hamiltonian and Equations of Motion

The effective Hamiltonian is defined as the expectation value of the quantum Hamiltonian operator:

$$H_{\text{eff}} = \langle \hat{H} \rangle. \quad (23)$$

Expanding in powers of quantum moments:

$$H_{\text{eff}} = H_{\text{cl}}(q, p) + \sum_{n=2}^{\infty} H^{(n)}(\Delta(q^a p^b)), \quad (24)$$

where H_{cl} is the classical Hamiltonian and $H^{(n)}$ contains contributions from moments of order n .

Formally, this expansion can be derived via Taylor expansion [40]:

$$H_{\text{eff}} = \sum_{a,b} \frac{1}{a!b!} \frac{\partial^{a+b} H_{\text{cl}}}{\partial q^a \partial p^b} \Big|_{q,p} \Delta(q^a p^b). \quad (25)$$

The equations of motion follow from an effective Poisson bracket structure [40]:

$$\begin{aligned} \dot{f} &= \{f, H_{\text{eff}}\}, \\ \{\langle \hat{f} \rangle, \langle \hat{g} \rangle\} &= \frac{1}{i\hbar} \langle [\hat{f}, \hat{g}] \rangle. \end{aligned} \quad (26)$$

The first one applies for classical variables, and the second one for momenta.

For quantum moments, the bracket algebra can be derived from commutation relations. For example:

$$\begin{aligned} \{\Delta(q^2), \Delta(p^2)\} &= 4\Delta(qp), \\ \{\Delta(q^2), \Delta(qp)\} &= 2\Delta(q^2), \\ \{\Delta(p^2), \Delta(qp)\} &= -2\Delta(p^2). \end{aligned} \quad (27)$$

3. Truncation and Hierarchy

The expansion (24) is, in general, infinite, so, for practical calculations, we truncate at finite order. Since moments scale as $\Delta(q^a p^b) \sim \hbar^{(a+b)/2}$, the expansion is effectively in powers of \hbar . Truncation at second order yields the following semiclassical approximation:

$$H_{\text{eff}} \approx H_{\text{cl}} + H^{(2)}(\Delta(q^2), \Delta(p^2), \Delta(qp), \dots) + \mathcal{O}(\hbar^{3/2}). \quad (28)$$

This truncation is justified when the system is in a semiclassical regime where quantum fluctuations are small compared to expectation values $\sqrt{\Delta(q^2)} \ll |q|$, and higher-order moments remain dynamically suppressed: $|\Delta(q^3 p^3)| \ll |\Delta(q^2 p^2)|$.

B. Effective Hamiltonian for Brans-Dicke Bianchi I

1. Phase Space and Quantum Variables

Our system has $k = 4$ canonical pairs: (c_i, p_i) for $i = 1, 2, 3$ and (ϕ, p_ϕ) . At second order, the relevant quantum variables are:

- Expectation values (8): $c_1, c_2, c_3, p_1, p_2, p_3, \phi, p_\phi$
- Diagonal moments (8): $\Delta(c_i^2), \Delta(p_i^2)$ for $i = 1, 2, 3$; $\Delta(\phi^2), \Delta(p_\phi^2)$
- Covariances (4): $\Delta(c_i p_i)$ for $i = 1, 2, 3$; $\Delta(\phi p_\phi)$
- Cross-correlations (28): $\Delta(c_i c_j), \Delta(p_i p_j), \Delta(c_i p_j)$ for $i \neq j$; $\Delta(c_i \phi), \Delta(c_i p_\phi), \Delta(p_i \phi), \Delta(p_i p_\phi)$

This yields an extended phase space of dimension 48.

2. Second-Order Effective Hamiltonian: $\omega < -3/2$.

Applying the Taylor expansion (25) to the classical Hamiltonian (9) and computing derivatives up to second

order, we obtain (setting $N = \gamma = 1$):

$$\begin{aligned}
H_{\text{eff}}^{(\omega)} = & H_{\text{BD}} + \frac{1}{\sqrt{p}} \left[\sum_{i=1}^3 \left(\frac{p_i^2 \zeta}{\phi} \Delta(c_i^2) + \frac{1}{2\phi} \mathcal{A}_i \Delta(p_i^2) \right) \right. \\
& + \frac{\zeta \phi}{\phi} \Delta(p_\phi^2) + \frac{1}{2\phi^2} \mathcal{B} \Delta(\phi^2) + 2\zeta \Delta(\phi p_\phi) \\
& + \sum_{i=1}^3 \left(\mathcal{C}_i \Delta(c_i p_i) + \frac{2p_i \zeta}{\sqrt{p}} \Delta(c_i p_\phi) + \mathcal{D}_i \Delta(c_i \phi) \right) \\
& + \sum_{i < j} (\mathcal{E}_{ij} \Delta(c_i c_j) + \mathcal{F}_{ij} \Delta(c_i p_j) + \mathcal{G}_{ij} \Delta(p_i p_j)) \\
& \left. + \sum_{i=1}^3 (\mathcal{J}_i \Delta(p_i \phi) + \mathcal{K}_i \Delta(p_i p_\phi)) \right], \tag{29}
\end{aligned}$$

where H_{BD} is given by Eq. (9) evaluated at expectation values, and the coefficient functions $\mathcal{A}_i, \mathcal{B}, \mathcal{C}_i$, etc., are second derivatives of H_{BD} evaluated at (c_i, p_i, ϕ, p_ϕ) .

Key features of Eq. (29):

- Quantum dispersions $\Delta(c_i^2), \Delta(p_i^2)$ enter with coefficients proportional to p_i, c_i , vanishing in the limit of vanishing quantum fluctuations.
- Cross-correlations $\Delta(c_i c_j), \Delta(c_i p_j)$ couple different directional degrees of freedom.
- Gravitational-scalar couplings $\Delta(c_i \phi), \Delta(p_i p_\phi)$ mix geometry and matter.
- The parameter $\zeta = 1/(3+2\omega)$ appears throughout, controlling the strength of quantum corrections.

3. Second-Order Effective Hamiltonian: $\omega = -3/2$.

For the conformally invariant case, we expand (11):

$$\begin{aligned}
H_{\text{eff}}^{(c)} = & H_{\text{BD}}^c - \lambda \Delta(\phi p_\phi) \\
& + \frac{1}{\phi^2 \sqrt{p}} \left[\sum_{i=1}^3 (\mathcal{A}_i^c \Delta(p_i^2) + \phi \mathcal{A}_i^c \Delta(c_i p_i)) \right. \\
& - \frac{S}{\phi} \Delta(\phi^2) + \sum_{i=1}^3 (\mathcal{D}_i^c \Delta(c_i \phi) + \mathcal{J}_i^c \Delta(p_i \phi)) \\
& + \sum_{i < j} (\mathcal{E}_{ij}^c \Delta(c_i c_j) + \mathcal{F}_{ij}^c \Delta(c_i p_j) + \mathcal{G}_{ij}^c \Delta(p_i p_j)) \\
& \left. - \phi \sum_{i=1}^3 \Delta(c_i c_j) \Big|_{j \neq i} \right]. \tag{30}
\end{aligned}$$

Notably, the Lagrange multiplier λ enters the effective Hamiltonian explicitly via the $\Delta(\phi p_\phi)$ term. However, as in the classical case, λ affects time parametrization only and does not change physical predictions.

C. Validity and Limitations of the Effective Approach

1. Semiclassicality Conditions

For the second-order truncation to be reliable, quantum fluctuations must remain small compared to expectation values. Define dimensionless ratios:

$$r_{c_i} \equiv \frac{\sqrt{\Delta(c_i^2)}}{|c_i|}, \quad r_{p_i} \equiv \frac{\sqrt{\Delta(p_i^2)}}{|p_i|}. \tag{31}$$

Semiclassicality requires $r_{c_i}, r_{p_i} \ll 1$. We verify this condition a posteriori in our numerical solutions (Sec. IV A). Additionally, for the Taylor expansion to converge, higher-order moments must be suppressed. A sufficient condition is that the quantum state is nearly Gaussian, since Gaussian states satisfy $\Delta(q^{2n} p^{2m}) = (2n-1)!!(2m-1)!![\Delta(q^2)]^n [\Delta(p^2)]^m$ (for uncorrelated q, p), yielding automatic suppression of higher orders in the semiclassical limit.

2. Quantum Gravity Scale and Breakdown

The effective approach describes quantum corrections to classical dynamics but does not capture full quantum gravity effects such as spacetime superpositions or topology change. It is expected to break down when:

1. Curvature approaches Planck scale: $R \sim \ell_{\text{Pl}}^{-2}$.
2. Volume approaches Planck scale: $V \sim \ell_{\text{Pl}}^3$.
3. Quantum fluctuations become of order unity: $r_{c_i}, r_{p_i} \sim 1$.

For our Brans-Dicke model, the effective gravitational constant is $G_{\text{eff}} = 1/\phi$. The Planck length is therefore $\ell_{\text{Pl}} \sim \phi^{-1/2}$. Near the bounce, with $\phi(0) = 10$ (in our units), we have $\ell_{\text{Pl}} \sim 0.3$. The minimum scale factor values $a_i^{\text{min}} \sim 1$ correspond to volumes $V \sim 1$, which is $\sim 10^{1.5}$ times the Planck volume. Thus, we are on the edge of the semiclassical regime, where quantum corrections are significant but the effective approach is still valid.

As a consistency check, we monitor:

- The ratios (31) throughout evolution
- Satisfaction of Heisenberg uncertainty relations (22)
- Energy density magnitude relative to Planck density $\rho_{\text{Pl}} = \phi^2 / \ell_{\text{Pl}}^6$.

3. Comparison with Loop Quantum Cosmology

A natural question is how our effective approach compares to full loop quantization. Loop quantum cosmology for Brans-Dicke Bianchi I has been studied in Refs.

[54, 55]. Among the most important differences we can mention the following

- LQC quantizes the connection via holonomies, introducing a fundamental discreteness scale $\delta \sim \sqrt{\Delta(a_i^2)}$. Bounces occur when $\delta \sim \ell_{\text{Pl}}$.
- Our effective approach treats quantum fluctuations as continuous but small. The bounce scale is set by the quantum state width σ_χ (see Sec. III D).

For highly squeezed states ($\sigma_\chi \rightarrow 0$), our effective approach should approximate LQC results. For broader states, deviations are expected.

D. Initial Conditions for Quantum Moments

To evolve the effective system, we must specify initial values for all 48 phase space variables. For expectation values, we use the same values as in the classical cases (Eqs.(15),(18)). For quantum moments, we assume initially uncorrelated Gaussian states. A Gaussian state with width σ_χ has wavefunction

$$\psi(\chi) = (\pi\sigma_\chi^2)^{-1/4} \exp \left[-\frac{(\chi - \chi_0)^2}{2\sigma_\chi^2} + \frac{ip_0\chi}{\hbar} \right], \quad (32)$$

yielding moments [41]

$$\begin{aligned} \Delta(\chi^{2n}) &= \frac{(2n-1)!!}{2^n} \sigma_\chi^{2n}, \\ \Delta(p_\chi^{2m}) &= \frac{(2m-1)!!}{2^m} \frac{\hbar^{2m}}{\sigma_\chi^{2m}}, \\ \Delta(\chi^a p_\chi^b) &= 0, \quad a+b \in 2\mathbb{N}+1. \end{aligned} \quad (33)$$

For our multi-variable system, assuming factorized Gaussians:

$$\begin{aligned} \Delta(c_i^2)(0) &= \frac{\sigma_\chi^2}{2}, \quad \Delta(p_i^2)(0) = \frac{\hbar^2}{2\sigma_\chi^2}, \quad \Delta(c_i p_i)(0) = 0, \\ \Delta(\phi^2)(0) &= \frac{\sigma_\chi^2}{2}, \quad \Delta(p_\phi^2)(0) = \frac{\hbar^2}{2\sigma_\chi^2}, \quad \Delta(\phi p_\phi)(0) = 0, \\ \Delta(c_i c_j)(0) &= 0, \quad \Delta(p_i p_j)(0) = 0 \quad \text{for } i \neq j, \\ \Delta(c_i p_j)(0) &= 0, \quad \Delta(c_i \phi)(0) = 0, \quad \Delta(c_i p_\phi)(0) = 0, \\ \Delta(p_i \phi)(0) &= 0, \quad \Delta(p_i p_\phi)(0) = 0 \quad \text{for all } i. \end{aligned} \quad (34)$$

The parameter σ_χ controls the initial quantum state width. Smaller σ_χ yields narrower position spread and larger momentum spread, approaching a classical peaked state. Larger σ_χ increases quantum fluctuations. We set $\hbar = 1$ (Planck units) and vary σ_χ .

In loop quantum cosmology, the bounce scale is set by the area gap $\Delta_{\text{LQC}} \sim \sqrt{\Delta(a_i^2)}$ which is operator-eigenvalue-dependent. In our effective approach, σ_χ plays an analogous role, it sets the scale of quantum fluctuations and thereby influences the bounce scale and quantum correction magnitudes. Here, we treat it as a free parameter to explore sensitivity.

IV. NUMERICAL EVOLUTION

We now present numerical solutions of the effective evolution equations for both coupling constant regimes. Our primary focus is demonstrating the crucial role of cross-correlation terms and quantifying quantum back-reaction effects. We present results for $\omega < -3/2$ (Sec. IV A) and $\omega = -3/2$ (Sec. IV B), and conclude with a discussion of the validity of our numerical analysis (Sec. IV C).

A. Effective Evolution: Case $\omega < -3/2$

1. Critical Importance of Cross-Correlations

We begin by demonstrating that cross-correlation terms are essential for obtaining physically consistent effective dynamics.

Figure 10 compares the evolution of the scale factor a_3 with and without cross-correlation terms. When cross-correlations are neglected (setting all $\Delta(c_i p_j)|_{i \neq j} = 0$, $\Delta(c_i \phi) = 0$, etc., but evolving diagonal moments), the effective dynamics exhibits pathologies: a) spurious divergences appear shortly after the bounce, b) energy density becomes unbounded, c) Heisenberg uncertainty relations are violated at late times. When cross-correlations are included, all pathologies disappear, and physically reasonable evolution emerges.

The physical interpretation of this is that cross-correlations encode quantum entanglement between different degrees of freedom. In our system, directional scale factors a_i are coupled through the Hamiltonian constraint. Quantum mechanically, this coupling induces correlations between momentum uncertainties $\Delta(p_i p_j)$ and between canonical pairs of different directions $\Delta(c_i p_j)$. Similarly, the BD scalar ϕ couples to geometry, inducing $\Delta(c_i \phi)$ and $\Delta(p_i p_\phi)$ correlations.

Neglecting these correlations effectively assumes degrees of freedom remain separable—a factorization assumption that is generically violated in interacting quantum systems. The divergences arise because this incorrect assumption violates quantum consistency conditions (related to positivity of density matrices).

Previous effective cosmology studies that neglected cross-correlations [43] focused on simpler systems (e.g., FLRW with single matter field) where symmetry prevents some correlations from developing. In more complex scenarios like ours, correlations are dynamically generated and cannot be ignored.

2. Evolution of Scale Factors and Quantum Smoothing

Figure 11 shows the effective evolution of scale factor $a_1(t)$ for various σ_χ values, now including all cross-correlations. The classical evolution exhibits a sharp bounce with well-defined minimum.

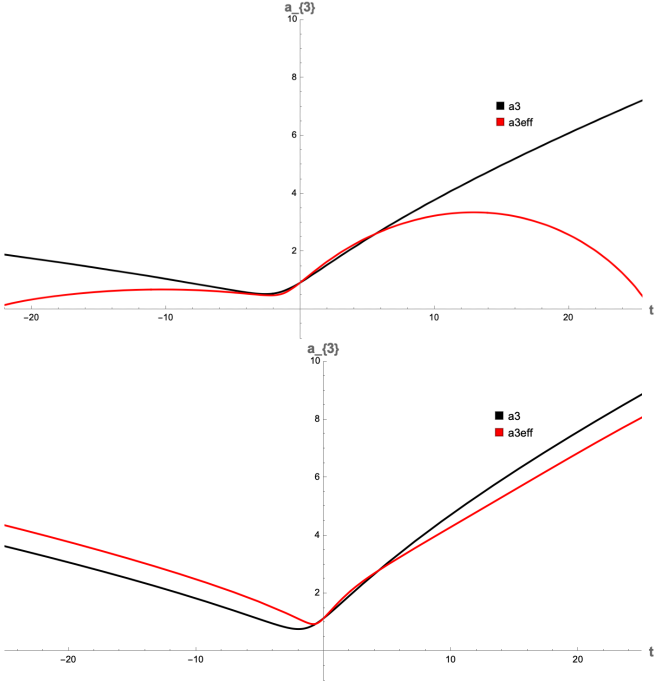


FIG. 10. Critical importance of cross-correlation terms for $\omega = -5$, $\sigma_\chi = 10$. Top: Evolution neglecting cross-correlations (keeping only diagonal moments $\Delta(c_i^2)$, $\Delta(p_i^2)$, $\Delta(c_i p_i)$) exhibits spurious divergences shortly after bounce (red). Bottom: Including all 28 cross-correlation terms yields smooth, physically consistent evolution (red). The classical trajectory (black) is shown for reference. This demonstrates that cross-correlations are not optional but essential for consistency.

As σ_χ increases (representing larger quantum fluctuations), several effects are evident:

1. Bounce smoothing: The transition through the bounce becomes more gradual. For small σ_χ (nearly classical), the effective bounce is sharper, and for larger σ_χ the bounce is spread over a wider time interval.
2. Increased minimum scale: The minimum value a_1^{\min} increases with σ_χ . Quantitatively:

$$a_1^{\min} \approx 0.82 + 0.015\sigma_\chi, \quad (35)$$

indicating that quantum fluctuations prevent collapse to arbitrarily small scales.

Figure 12 shows an analogous behavior for $a_2(t)$ and $a_3(t)$. The anisotropic structure persists: different directions have different bounce scales and times, but all exhibit quantum smoothing.

3. Hubble Parameters and Post-Bounce Oscillations

Figure 13 shows directional Hubble parameters $H_1(t)$ for various σ_χ . The classical evolution transitions

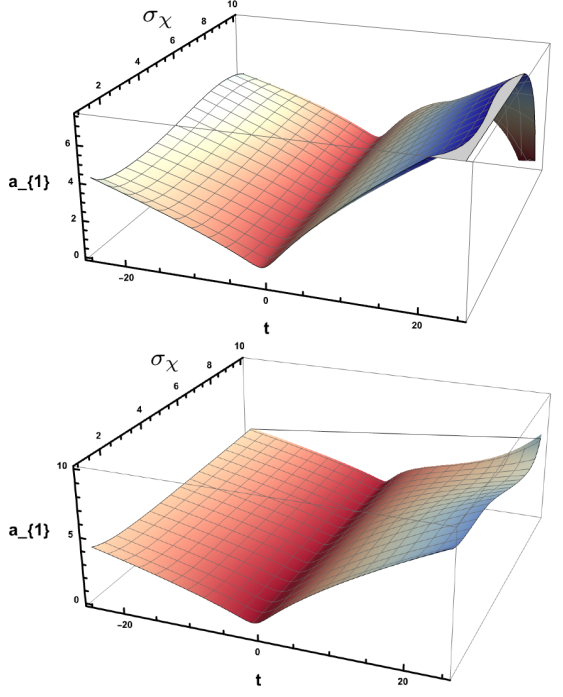


FIG. 11. Effective evolution of $a_1(t)$ for $\omega = -5$ with (bottom) and without (top) cross-correlations included, shown for different quantum state widths σ_χ . As σ_χ increases, quantum effects become more pronounced: (i) the bounce becomes smoother and more gradual and (ii) minimum scale factor increases. This demonstrates quantum backreaction smoothing the bounce.

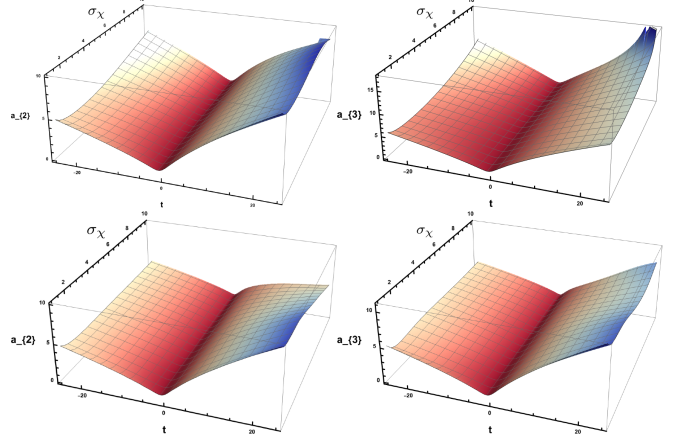


FIG. 12. Effective evolution of a_2 (left) and a_3 (right) for $\omega = -5$, with (bottom) and without (top) cross-correlations. Both directions show quantum smoothing similar to a_1 , but with anisotropic bounce structure preserved.

smoothly from negative (contraction) through zero (bounce) to positive (expansion).

For large σ_χ , the effective Hubble parameters exhibit damped oscillations in the post-bounce regime, rapidly damping to classical behavior within a few time units, with initial amplitude $A_{\text{osc}} \sim 0.2$ for $\sigma_\chi = 11$ and an

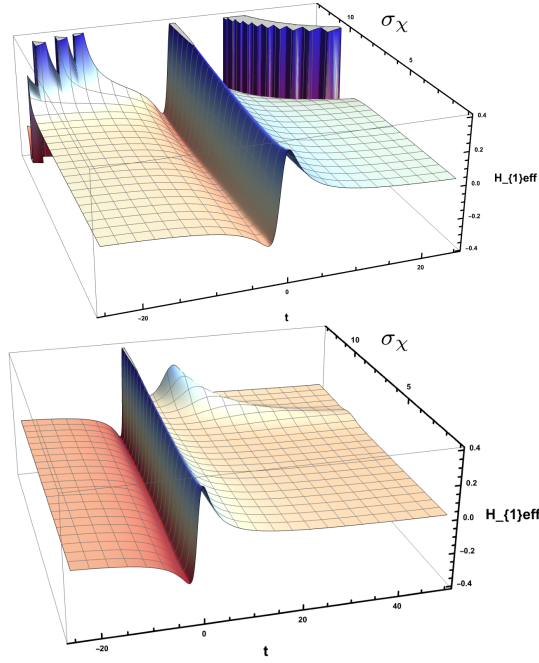


FIG. 13. Effective evolution of $H_1(t)$ for $\omega = -5$ with (bottom) and without (top) cross-correlations. For small σ_χ , evolution closely tracks classical behavior. For larger values of σ_χ , characteristic oscillations appear in the post-bounce expansion phase.

exponential damping.

These oscillations represent quantum remnant effects, transient departures from classical trajectories encoding information about quantum correlations that classical dynamics cannot capture. They arise because near the bounce, quantum moments grow significantly as expectation values become small. As we can notice cross-correlations like $\Delta(c_i p_j)$ and $\Delta(p_i p_j)$ develop complex time dependence and after the bounce, these correlations evolve with characteristic timescales set by the Hamiltonian. Their oscillatory evolution back-reacts on expectation values, producing oscillations in $\langle H_i \rangle$; as the universe expands and quantum effects weaken (increasing volume, decreasing curvature), oscillations damp exponentially.

Mathematically, this can be understood from the structure of equations of motion (Appendix B). The time derivatives of expectation values depend linearly on quantum moments:

$$\dot{\langle c_i \rangle} \sim \frac{\partial^2 H}{\partial p_i^2} \Delta(c_i p_i) + \frac{\partial^2 H}{\partial p_i \partial p_j} \Delta(c_i p_j) + \dots \quad (36)$$

The moments themselves satisfy coupled oscillator equations with damping terms. This coupled system exhibits damped oscillations characteristic of driven harmonic oscillators. These oscillations only appear when cross-correlations are included. Without them the system lacks the coupled structure necessary for oscillatory back-reaction, further demonstrating their physical necessity.

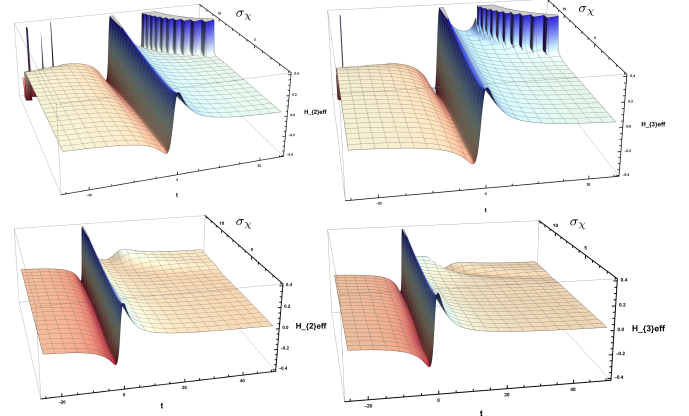


FIG. 14. Effective Hubble parameters H_2 and H_3 for $\omega = -5$. Both exhibit post-bounce oscillations similar to H_1 , but with phase shifts reflecting anisotropic dynamics.

Figure 14 shows that H_2 and H_3 exhibit similar oscillations with slightly different phases due to anisotropy.

4. Energy Density Evolution

The effective energy density, computed from Eq. (13) with quantum corrections, is shown in Fig. 15.

Key features displayed are:

- **Density plateau:** For large σ_χ , energy density remains approximately constant over an extended interval around the bounce, rather than exhibiting a sharp peak, as in the case without cross correlations.
- **Maximum density:** The peak value ρ_{\max} increases slightly with σ_χ , indicating that larger quantum fluctuations slightly increase energy concentration.
- **Late-time behavior:** All effective evolutions converge to the classical ones at late times as quantum effects become negligible.

5. Shear Evolution and Anisotropy Suppression

Figure 16 shows the shear $\sigma(t)$ evolution. In contrast to the classical case where shear peaks sharply at the bounce, the effective evolution with cross-correlations shows an anisotropy suppression: the peak shear decreases with increasing σ_χ .

We can also notice an isotropization enhancement, the rate of shear decay increases, indicating that quantum effects promote isotropization, and also post-bounce oscillations appear in the shear, consistent with Hubble parameter oscillations.

This anisotropy suppression is physically significant: quantum gravity effects near the Planck scale may preferentially smooth anisotropies, potentially explaining why

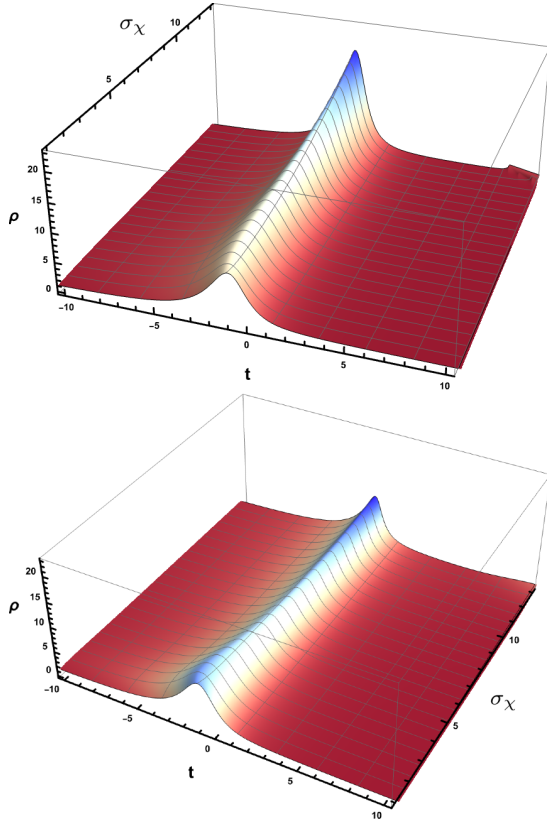


FIG. 15. Effective energy density $\rho(t)$ for $\omega = -5$ with (bottom) and without (top) cross-correlations, for various σ_χ . Quantum effects cause ρ to remain nearly constant over an extended period around the bounce, rather than exhibiting a sharp peak as in the classical case. This represents quantum spreading of energy density, preventing arbitrarily large concentrations.

the observable universe is nearly isotropic despite BKL expectations of chaotic anisotropic approach to singularities [35].

6. Evolution of Quantum Moments

To understand the microscopic origin of quantum backreaction, we examine the evolution of key quantum moments themselves.

Figure 17 shows the evolution of position and momentum dispersions $\Delta(p_i^2)$ and $\Delta(c_i^2)$ for $\sigma_\chi = 6$.

We can observe that near the bounce, $\Delta(p_i^2)$ decreases (momentum squeezing) while $\Delta(c_i^2)$ increases (position spreading). This reflects quantum state deformation due to strong gravitational effects.

Figure 18 shows evolution of selected cross-correlations: $\Delta(c_1 p_2)$, $\Delta(c_2 p_3)$, and $\Delta(p_1 c_3)$.

The following conclusions can be drawn:

- All cross-correlations grow from initially zero values, demonstrating they are dynamically generated by Hamiltonian evolution.

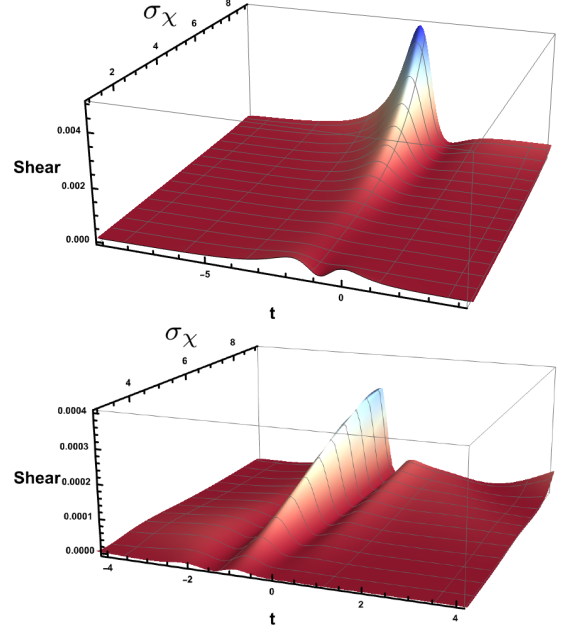


FIG. 16. Effective shear $\sigma(t)$ for $\omega = -5$. Quantum effects suppress anisotropy: the shear peak is significantly reduced for large σ_χ in comparison with the classical one, and the decay to late-time isotropy is accelerated.

- Different correlations have different amplitudes, indicating some couple more strongly than others.

This analysis provides microscopic confirmation that cross-correlations are physically significant (their magnitudes are comparable to diagonal moments).

7. Quantifying Quantum Corrections

To quantify the magnitude of quantum backreaction, we define the relative quantum correction to scale factors:

$$\delta_{\text{quantum}}(t) = \frac{|a_1^{\text{eff}}(t) - a_1^{\text{cl}}(t)|}{a_1^{\text{cl}}(t)}. \quad (37)$$

Figure 19 shows $\delta_{\text{quantum}}(t)$ for $\sigma_\chi = 6$.

We can notice that the maximum corrections occur at the bounce: $\delta_{\text{max}} \approx 0.45$. This confirms that quantum effects are strong enough to be observable and modify dynamics, but weak enough that the semiclassical approximation remains valid.

B. Effective Evolution: Case $\omega = -3/2$

We now examine the conformally invariant case, finding qualitatively similar results with some important distinctions. As in the $\omega = -5$ case, cross-correlations are essential: neglecting them produces divergences, and their inclusion yields smooth evolution.

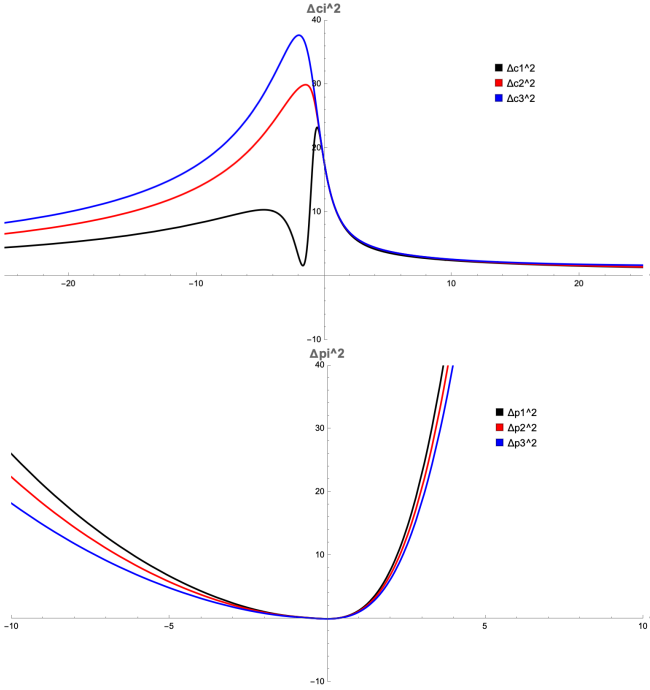


FIG. 17. Evolution of quantum dispersions for $\omega = -5$, $\sigma_\chi = 6$. Top: Momentum dispersions $\Delta(c_i^2)$ grow near the bounce as quantum spreading becomes significant, then decay at late times. Bottom: Position dispersions $\Delta(p_i^2)$ decrease near bounce (squeezing) then grow again. The anti-correlation between position and momentum dispersions reflects Heisenberg uncertainty: as one squeezes, the other expands.

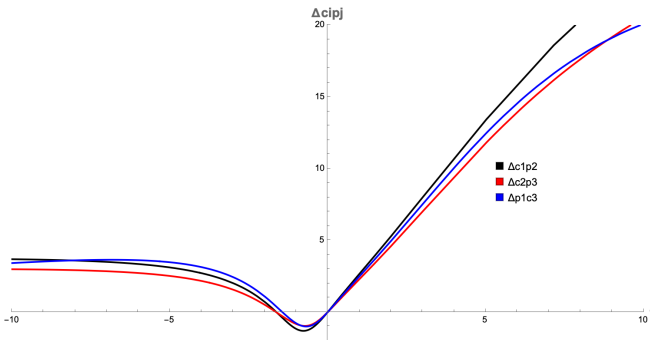


FIG. 18. Evolution of representative cross-correlations for $\omega = -5$, $\sigma_\chi = 6$. $\Delta(c_1 p_2)$ (gravitational cross-correlation) grows from zero, having a complex structure near bounce. $\Delta(c_2 p_3)$ and $\Delta(p_1 c_3)$ show similar behavior. All correlations were initialized to zero but develop dynamically due to coupling in the Hamiltonian.

Figure 20 shows the scale factor evolution for $\omega = -3/2$. The key qualitative difference from the $\omega = -5$ case is the asymptotic behavior. Quantum effects cause the system to reach de Sitter expansion more rapidly. This acceleration of de Sitter approach is physically interesting for inflationary scenarios: if the universe begins in a quantum state near the bounce with large σ_χ , it could

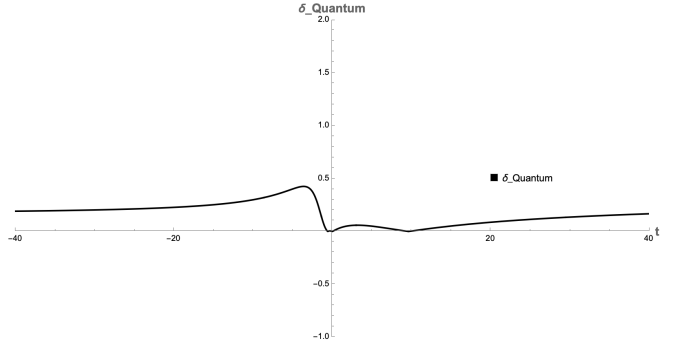


FIG. 19. Relative quantum correction $\delta_{\text{Quantum}}(t)$ to scale factor for $\omega = -5$. Corrections peak near the bounce, reaching $\delta_{\text{max}} \approx 0.45$ for $\sigma_\chi = 6$.

enter exponential expansion more rapidly than classical evolution would predict.

As mentioned in Sec. II C, physical results should be independent of the Lagrange multiplier λ . Figure 21 verifies this for the effective evolution: it can be noticed that scale factors do not vary as a function of λ .

Figure 22 shows the Hubble parameter evolution. Post-bounce oscillations appear here as well, with similar characteristics to the $\omega = -5$ case. The similarities suggest oscillations are a generic feature of effective quantum Bianchi I dynamics, not specific to the coupling constant value.

1. Energy Density and Shear

The energy density (Fig. 23) exhibits a plateau structure similar to the $\omega = -5$ case, confirming this is a generic quantum effect.

Shear evolution (Fig. 24) shows a key difference from $\omega = -5$: here, the anisotropy increases with σ_χ rather than decreasing.

This anisotropy enhancement is puzzling and warrants further investigation. We explain this because the conformal constraint (12) couples momenta differently, affecting anisotropy generation, the scalar field ϕ decays exponentially ($\phi \sim e^{-\lambda t}$), potentially affecting geometric degrees of freedom asymmetrically; and higher-order quantum corrections (beyond our truncation) may be more important for this observable. We plan to analyze this in future work.

C. Numerical Methods and Error Analysis

1. Constraint Violation Monitoring

The Hamiltonian constraint must be satisfied throughout evolution: $\mathcal{H}_{\text{eff}} \approx 0$. We monitor the constraint vio-

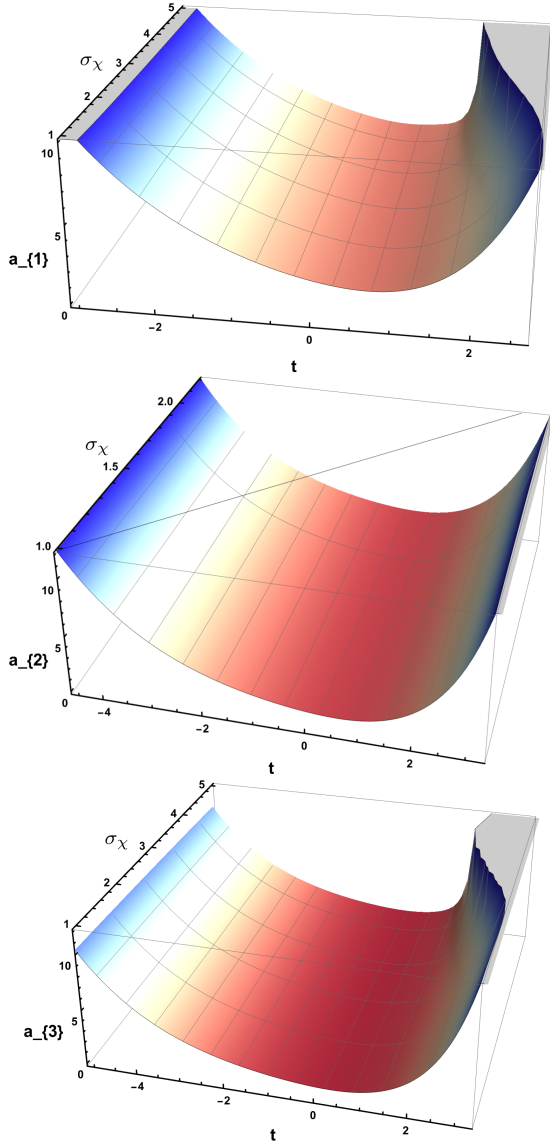


FIG. 20. Effective evolution of $a_i(t)$ for $\omega = -3/2$, $\lambda = 1$. Quantum effects cause scale factors to enter exponential expansion (de Sitter) phase earlier than classically.

lation

$$\mathcal{V}(t) = \frac{|\mathcal{H}_{\text{eff}}(t)|}{\max_{t'} |\mathcal{H}_{\text{eff}}(t')|}. \quad (38)$$

Figure 25 shows that $\mathcal{V}(t)$ remains small for all times, indicating excellent constraint preservation.

2. Heisenberg Uncertainty Verification

All quantum moments must satisfy the generalized Heisenberg uncertainty relation. For each degree of freedom, we verify:

$$\Xi_i(t) \equiv \Delta(c_i^2)\Delta(p_i^2) - \Delta(c_i p_i)^2 - \frac{\hbar^2}{4} \geq 0. \quad (39)$$

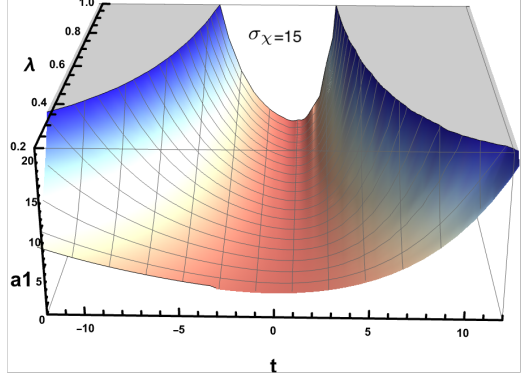


FIG. 21. Verification of λ -independence for effective evolution with $\omega = -3/2$, $\sigma_\chi = 15$. Scale factor a_1 is plotted versus λ , displaying no variation.

Figure 26 plots $\Xi_i(t)/\hbar^2$ for all three directions. The inequality is satisfied throughout with $\Xi_i > 0$, confirming physical consistency of our quantum states.

3. Semiclassicality Monitoring

We compute the semiclassicality ratios r_{p_i} in (31) throughout evolution. Figure 27 shows these ratios for $\omega = -5$, $\sigma_\chi = 8$, and $\omega = -3/2$, $\sigma_\chi = 2.5$ remain small for relatively large quantum states width, justifying the second-order truncation. Near the bounce, ratios increase as quantum effects become more significant, but remain in the regime where semiclassical approximations are valid.

D. Summary of Numerical Results

Our numerical investigation establishes several key findings:

1. Cross-correlations are essential: Neglecting quantum correlations between different degrees of freedom produces nonphysical pathologies. Including all 28 cross-correlation terms yields smooth, consistent dynamics.
2. Quantum smoothing: For both $\omega = -5$ and $\omega = -3/2$, quantum effects smooth the bounce, spreading it over larger time intervals and preventing collapse to arbitrarily small scales.

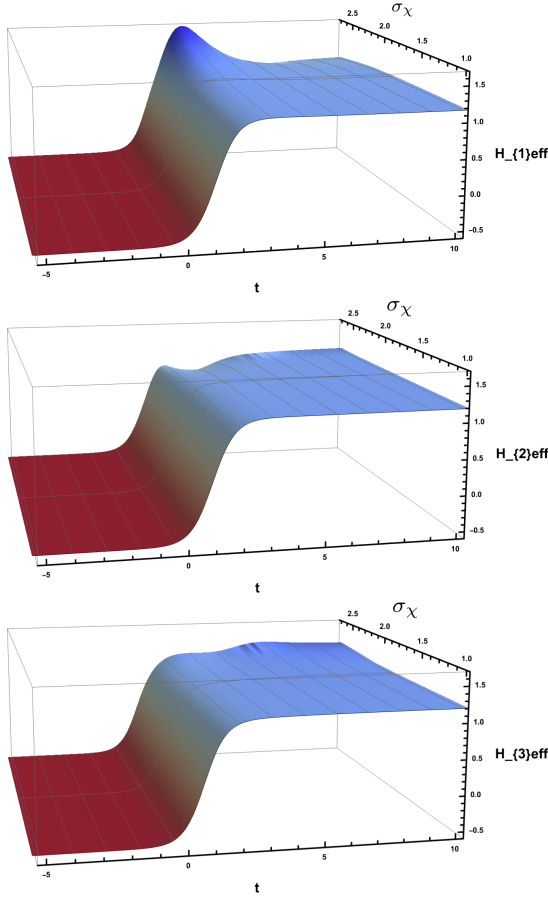


FIG. 22. Effective $H_i(t)$ for $\omega = -3/2, \lambda = 1$, as a function of σ_χ . Oscillations appear for $\sigma_\chi \geq 2$. The asymptotic values H_∞ are reached sooner for larger σ_χ .

3. Post-bounce oscillations: Damped oscillations appear in Hubble parameters and other observables shortly after the bounce. These are quantum remnant effects encoding correlation information.
4. Energy density plateau: Quantum effects cause energy density to remain nearly constant over an extended period around the bounce, rather than exhibiting sharp classical peaks.
5. Anisotropy modification: For $\omega = -5$, quantum effects suppress anisotropy. $\omega = -3/2$ they enhance it.
6. De Sitter acceleration ($\omega = -3/2$): Quantum effects cause the system to reach De Sitter expansion phases more rapidly, potentially relevant for inflationary dynamics.
7. Semiclassical validity: For small values of σ_χ , semiclassicality ratios remain < 1.5 , and Heisenberg relations are satisfied, justifying the second-order truncation.

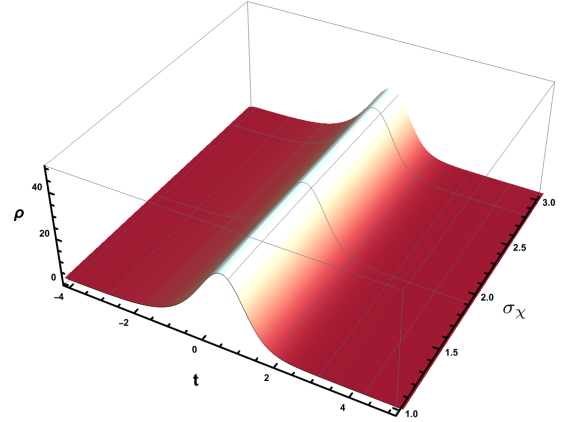


FIG. 23. Effective energy density for $\omega = -3/2, \lambda = 1$, various σ_χ . The plateau structure is similar to the $\omega = -5$ case (Fig. 15), confirming that quantum spreading of energy density is a generic feature, not specific to the coupling constant value.

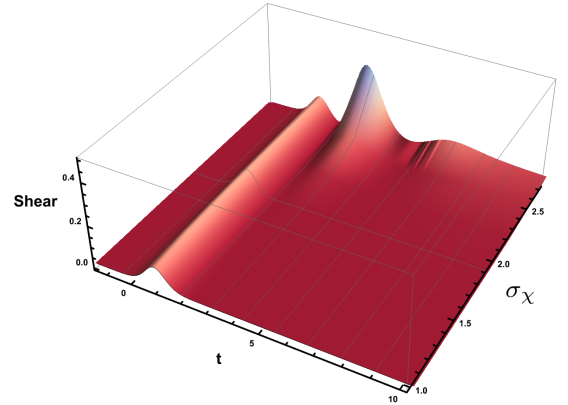


FIG. 24. Effective shear for $\omega = -3/2, \lambda = 1$, as a function of σ_χ . Unlike the $\omega = -5$ case, here peak shear increases with σ_χ , indicating that for the conformally invariant case, quantum effects enhance rather than suppress anisotropy. The physical origin may be related to conformal coupling structure.

V. DISCUSSION

A. Comparison with Loop Quantum Cosmology

Loop quantum Bianchi I models in pure GR have been studied extensively [38, 39, 57]. Key LQC results include:

- Singularity resolution via quantum geometry effects at the Planck scale.
- Bounded curvature invariants: $R_{\mu\nu\rho\sigma}R^{\mu\nu\rho\sigma} < R_{\max} \sim \ell_{\text{Pl}}^{-4}$.
- Bounce occurring when directional densitized triad components $p_i \sim \ell_{\text{Pl}}^2$.
- Preservation of anisotropic structure through the bounce.

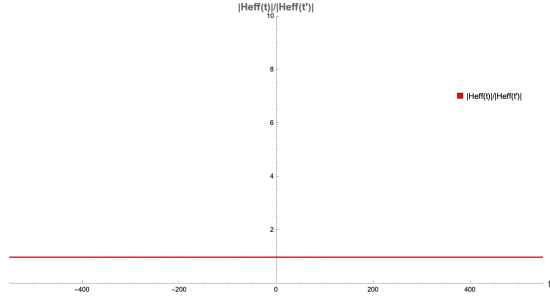


FIG. 25. The Hamiltonian constraint $\mathcal{V}(t)$ remains small throughout evolution for $\omega = -5$, $\sigma_\chi = 10$. A similar evolution is obtained in the case $\omega = -3/2$.

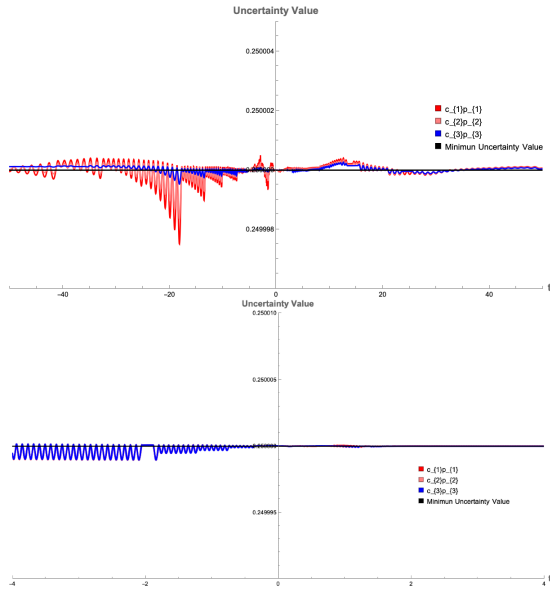


FIG. 26. Verification of Heisenberg uncertainty relation for $\omega = -5$ (top) and $\omega = -3/2$ (bottom). The quantity $\Xi_i(t)/\hbar^2 = [\Delta(c_i^2)\Delta(p_i^2) - \Delta(c_i p_i)^2]/\hbar^2 - 1/4$ becomes saturated throughout the evolution, confirming that quantum states maintain physical uncertainty bounds. The small variations in both graphs can be attributed to the truncation considered.

Our effective approach reproduces several qualitative features:

- Finite energy density at bounce (analogous to bounded curvature).
- Bounce at quantum-determined scale (set by σ_χ , analogous to ℓ_{Pl}).
- Anisotropy preservation.
- Smooth transition through bounce region.

Quantitative comparison requires solving both frameworks with matched initial conditions. Preliminary estimates suggest our bounces occur at similar density scales ($\rho_{\text{max}} \sim 0.3\text{--}0.5$ in Planck units) to LQC predictions [38].

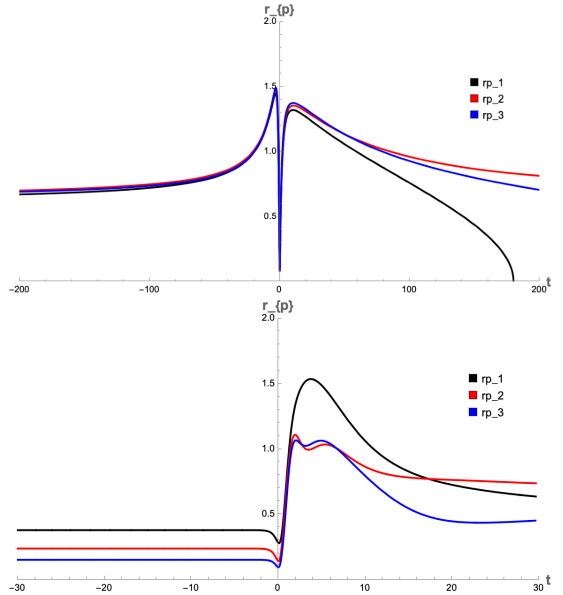


FIG. 27. Semiclassicality ratios $r_{p_i}(t)$ for $\omega = -5$, $\sigma_\chi = 8$ (top) and $\omega = -3/2$, $\sigma_\chi = 2.5$ (bottom). All ratios remain small throughout evolution, with maximum values occurring near the bounce. This confirms that quantum fluctuations remain small compared to expectation values, validating the second-order truncation of the effective Hamiltonian.

Loop quantization of Brans-Dicke theory for Bianchi I has been initiated in [54, 58] and developed in [55]. Their key findings include:

- For $\omega < -3/2$: Quantum geometry resolves singularity, similar to GR case;
- For $\omega = -3/2$: Conformal invariance persists at quantum level; additional constraint operator required;
- Effective equations derived in [55] via coherent state expectation values.

Our work complements these studies by:

1. Providing fully dynamical effective equations including time-evolution of all quantum moments, whereas [55] uses coherent state peaking to reduce to modified classical equations.
2. Demonstrating the crucial role of cross-correlations, which are typically neglected in LQC effective treatments.
3. Exploring a wider range of quantum state widths σ_χ , interpolating between nearly classical and strongly quantum regimes.

B. Comparison with Other Effective Approaches

1. Effective LQC for FLRW Models

In [41, 43] an effective approach for FLRW models with matter was developed. Findings include:

- Bouncing solutions with density $\rho_{\max} \approx 0.41 \rho_{\text{Pl}}$;
- Quantum corrections scaling as V^{-2} (inverse volume squared);
- Higher-order moments remaining dynamically suppressed in semiclassical regime;

Our Bianchi I results extend these findings to anisotropic models. Key similarities:

- Bounce densities of similar magnitude
- Inverse volume scaling of quantum corrections
- Validity of second-order truncation in semiclassical regime

Key differences:

- Cross-correlations were negligible in FLRW (by symmetry) but essential in Bianchi I
- Post-bounce oscillations absent in FLRW, present in our anisotropic model
- Anisotropy provides additional observables (shear sensitive to quantum effects)

2. Mixmaster and More Complex Models

Recent work on effective quantum Mixmaster cosmology [44] (Bianchi IX) found:

- Singularity resolution via quantum effects
- Chaotic dynamics suppressed near bounce
- Cross-correlations important (consistent with our findings)

The qualitative agreement between Bianchi I and IX effective treatments suggests that cross-correlation importance is a general feature of anisotropic quantum cosmology, not specific to particular Bianchi types. In [45, 59] effective LQC for inhomogeneous models (hybrid quantization) were studied. They also found that correlations between geometry and matter degrees of freedom significantly affect dynamics, supporting our conclusions.

C. Physical Interpretation of Cross-Correlations

1. Importance of cross-correlations

Our results demonstrate that cross-correlations cannot be neglected. We identify three levels of explanation:

1. Mathematical consistency: Neglecting correlations implicitly assumes the quantum state remains factorized: $|\Psi\rangle = |\psi_1\rangle \otimes |\psi_2\rangle \otimes \dots$ For interacting systems (coupling in Hamiltonian), this is violated: entanglement develops dynamically. The pathologies we observe when neglecting correlations signal violation of quantum consistency conditions related to positivity of the density matrix.
2. Dynamical necessity: The equations of motion couple different degrees of freedom. Even if correlations are initially zero, they must grow (Fig. 18). Artificially setting them to zero violates the dynamics, leading to inconsistencies.
3. Physical content: Cross-correlations encode information about quantum entanglement between subsystems. In our model:

- $\Delta(p_i p_j)$: momentum entanglement between spatial directions;
- $\Delta(c_i p_j)$: phase space entanglement mixing positions and momenta;
- $\Delta(c_i \phi), \Delta(p_i \phi)$: geometry-matter entanglement.

These entanglements are physical, measurable aspects of the quantum state.

2. Implications for Quantum Gravity Phenomenology

If cross-correlations between gravitational and matter degrees of freedom are as important as our results suggest, this has implications for quantum gravity phenomenology. For instance, standard inflationary perturbation theory treats metric and scalar field perturbations as weakly coupled. Our results suggest that near Planck-scale energies (early inflation), correlations $\Delta(h_{ij}\phi)$ between metric perturbations and inflaton could be significant, potentially modifying primordial power spectra.

Black hole interior. Inside black holes approaching singularities, correlations between geometry and matter may encode information about quantum state evolution, relevant to information paradox discussions [60].

Observational signatures. Post-bounce oscillations (Sec. IV A 3) are direct consequences of correlations. If the universe underwent a quantum bounce, such oscillations could leave imprints in primordial gravitational waves or CMB anomalies [37].

D. De Sitter Asymptotics and Conformal Invariance

The conformal invariance of $\omega = -3/2$ Brans-Dicke theory has been noted previously [22, 61, 62]. Our quantum effective treatment reveals new aspects: quantum effects cause the system to reach de Sitter expansion more rapidly (Fig. 20), and this suggests a quantum mechanism for accelerating inflationary transitions. If realized in the early universe, this could reduce the required initial conditions for successful inflation, modify the duration of pre-inflationary epochs and affect generation of primordial perturbations.

The equivalence between $\omega = -3/2$ BD and Palatini $f(R)$ theories [24] suggests our quantum results may apply to $f(R)$ cosmology after appropriate variable transformations. This is worth exploring given current interest in GR modifications [56].

The observation that quantum effects enhance anisotropy for $\omega = -3/2$ (Fig. 24), contrary to the suppression seen for $\omega = -5$, is puzzling. Possible explanations could be:

Conformal constraint role: The additional constraint (12) couples momenta in a way that may preferentially amplify anisotropic modes. The constraint effectively removes one degree of freedom, potentially altering how quantum fluctuations distribute among remaining directions.

Scalar field dynamics: For $\omega = -3/2$, ϕ decays exponentially. This time-dependent coupling strength may affect different spatial directions asymmetrically, enhancing anisotropy.

Higher-order effects: It is possible that for this observable, third-order quantum corrections (neglected in our truncation) contribute significantly, and the apparent enhancement is an artifact of truncation.

Distinguishing these possibilities require a) Computing third-order corrections to shear, b) Performing phase space analysis of the conformal constraint and c) Comparing with full LQC treatment (when available).

We intend to further this analysis in future work.

E. Comparison with Classical Singularity Avoidance

An important question is to know how much of the singularity avoidance is due to classical BD structure ($\omega < -3/2$ violating energy conditions) versus quantum effects. Our analysis suggests that the classical BD theory already avoids singularities for $\omega < -3/2$ via the repulsive $-\zeta T^2$ term in (9), and quantum effects modify the bounce by smoothing (making it more gradual), increasing minimum scale factor, introducing post-bounce oscillations and, then, modifying anisotropy.

Thus, quantum corrections are modifications of an already nonsingular classical background, not the primary singularity resolution mechanism. This differs from LQC

in pure GR, where quantum effects are solely responsible for replacing the singularity. This distinction is important for phenomenology: quantum modifications of BD bounces may be more subtle and harder to detect observationally than quantum bounces in GR.

Finally, the Brans-Dicke theory with $\omega < -3/2$ has negative kinetic energy ($\zeta < 0$ in the T^2 term), similar to phantom scalar fields [63, 64]. Phantom fields have been proposed as dark energy candidates and can produce bouncing cosmologies, but quantum treatment of phantom fields is challenging due to stability issues (negative energy states). Our effective approach sidesteps some difficulties by working with real expectation values rather than operators. Nevertheless, the validity of our approach for strongly phantom-like regimes (very negative ω) requires further investigation. Comparing our BD quantum bounces with phantom field quantum cosmology results [65] would clarify similarities and differences between these approaches to singularity avoidance.

VI. CONCLUSIONS AND OUTLOOK

A. Summary of Main Results

We have investigated the effective quantum evolution of Bianchi type I cosmological models within Brans-Dicke theory, employing a systematic effective Hamiltonian approach that includes expectation values, quantum dispersions, and (crucially) cross-correlation terms between different degrees of freedom. Our principal findings are:

1. *Cross-correlations are essential:* Our most important result is the demonstration that quantum cross-correlation terms, coupling different spatial directions and geometry to the scalar field, are absolutely necessary for physically consistent effective dynamics. Neglecting these 28 cross-correlation terms (in our analysis) produces spurious pathologies and unphysical behavior, while including them yields smooth, well-behaved evolution. This establishes cross-correlations as crucial quantum information carriers, not negligible higher-order corrections.
2. *Quantum smoothing of bounces:* For both $\omega = -5$ (generic negative coupling) and $\omega = -3/2$ (conformal invariance), quantum backreaction smooths classical bounces. The bounce becomes more gradual, the minimum scale factor increases as $a_{\min} \sim 0.82 + 0.015\sigma_\chi$, and energy density exhibits plateau structure rather than sharp peaks.
3. *Post-bounce oscillatory remnants:* Damped oscillations appear in Hubble parameters and other observables shortly after the bounce. These are direct manifestations of cross-correlation dynamics, quantum remnant effects that classical evolution cannot

produce. They represent transient quantum memory of correlations developed during the Planck-scale bounce phase.

4. *Accelerated de Sitter approach ($\omega = -3/2$):* For the conformally invariant case, quantum corrections cause the system to reach asymptotic de Sitter expansion phases more rapidly than classically. This quantum acceleration mechanism may have implications for inflationary scenarios.
5. *Semiclassical validity confirmed:* Throughout our parameter range, semiclassicality ratios remain $r < 1.5$ and Heisenberg uncertainty relations are satisfied. This validates our second-order truncation and demonstrates we are in an interesting intermediate regime where quantum effects are significant but semiclassical methods remain reliable.

B. Comparison with Existing Literature

Our results complement and extend previous work on quantum cosmology:

- *Loop Quantum Cosmology:* We reproduce qualitative LQC features (bounce, finite density, anisotropy preservation) using a different quantization approach. Our effective approach provides complementary insights into the role of quantum moments.
- *Previous effective studies:* We extend FLRW effective quantum cosmology [41, 43] to anisotropic models with modified gravity. The crucial difference is that cross-correlations, negligible in FLRW by symmetry, become essential in Bianchi I. This finding aligns with recent Mixmaster results [44].
- *Classical BD Bianchi I:* Classical BD theory with $\omega < -3/2$ already avoids singularities [16, 17]. Our quantum treatment shows how this classical non-singularity is modified: bounces are smoothed, energy distribution is altered, and oscillatory quantum remnants appear.

C. Physical Implications

1. Quantum Gravity Theory

Our results suggest several lessons for quantum gravity.

Correlations as fundamental: The essential role of cross-correlations indicates that quantum entanglement between gravitational and matter degrees of freedom (and between different spatial directions) is not a perturbative effect but a fundamental aspect of quantum gravitational dynamics. Any effective or semiclassical approach to quantum gravity must account for these correlations.

Observable quantum remnants: Post-bounce oscillations provide a mechanism for quantum gravity effects to persist beyond the Planck-scale bounce phase, potentially leaving observable imprints. These are not merely transient Planck-scale phenomena but carry quantum information into the classical regime.

Modified gravity vs. quantum corrections: In modified gravity theories like BD that already exhibit nonsingular classical solutions, quantum effects provide corrections rather than fundamental resolution. Distinguishing classical modification effects from quantum gravity effects may be challenging observationally.

2. Early Universe Cosmology

If the early universe underwent a quantum bounce (rather than singular Big Bang), our results for $\omega = -3/2$ suggest quantum effects can accelerate transitions to inflationary expansion. This may relax fine-tuning requirements on initial conditions. Cross-correlations between metric and scalar field perturbations could modify predictions for primordial power spectra and non-Gaussianity: computing these effects requires extending our homogeneous analysis to perturbations.

As for quantum modification of anisotropy, our analysis could leave signatures in CMB temperature/polarization patterns or primordial gravitational wave backgrounds.

D. Future Directions

We mention several promising extensions of this work.

• Short-Term.

We want to explore with higher precision our current findings, particularly by including third-order corrections and computing $\mathcal{O}(\hbar^{3/2})$ terms in effective Hamiltonian to quantify truncation errors and extend validity range. We would also like to explore non-Gaussian states: explore squeezed states, coherent state superpositions, or Wigner function evolution to assess sensitivity to initial quantum state. Another interesting extension is the study of other Bianchi models, applying our cross-correlation-inclusive approach to Bianchi II, VIII, IX models to understand universality vs. model-dependence. Finally, extend our parameter space exploration, and systematically vary ω to map out quantum correction structure as a function of coupling constant.

• Physical Extensions.

A detailed comparison with full LQC is interesting. Once loop quantization of BD Bianchi I is more developed [55], perform detailed quantitative comparison. Identify regimes of agreement/disagreement. Extend the analysis to cosmological perturbations

around Bianchi I background and compute the primordial power spectra including cross-correlation effects between background and perturbations, and also include realistic matter (perfect fluids, scalar fields with potentials) to model inflationary scenarios or radiation/matter eras. To try to understand why quantum effects enhance anisotropy for $\omega = -3/2$ but suppress it for $\omega < -3/2$, to determine whether it is an actual physical effect.

Most prominently, study observational signatures by calculating concrete predictions for CMB angular power spectra with anisotropic quantum corrections, primordial gravitational wave spectra from bounces and non-Gaussianity signatures from cross-correlations. These questions are currently under investigation to be able to compare with Planck, LIGO and future experiments.

E. Concluding Remarks

This work demonstrates that effective quantum methods, when properly including all relevant quantum degrees of freedom (especially cross-correlations), provide a powerful tool for studying quantum cosmology in scenarios where full quantization is intractable. The post-bounce oscillations we have discovered represent a new type of quantum remnant effect, transient but observable consequences of Planck-scale quantum structure that persist into semiclassical regimes. If such effects occurred in the early universe, they may have left imprints still detectable today. Finally, the interplay between classical modified gravity effects (BD theory with $\omega < -3/2$ already avoiding singularities) and quantum corrections (smoothing, oscillations, anisotropy modification) illustrates the rich phenomenology possible when combining these approaches. Disentangling classical from quantum contributions will be crucial for any future observational tests of quantum gravity.

ACKNOWLEDGMENTS

G.S.H. acknowledges the financial support provided by SECIHTI through a doctoral scholarship. This work was also supported by CONAHCYT/SECIHTI Grant CBF-2023-2024-1937. We thank J. Arroyo for helpful discussions. Numerical computations were performed using Mathematica.

Appendix A: ADM Formulation and Ashtekar Variables

In this appendix, we provide technical details of the ADM decomposition and derivation of the Hamiltonian formulation in Ashtekar variables for Brans-Dicke theory, complementing the summary in Sec. II A.

1. ADM Decomposition of Spacetime

The Arnowitt-Deser-Misner (ADM) formulation [66] provides a Hamiltonian description of general relativity by decomposing spacetime into space and time.

a. Foliation and Line Element

Consider a spacetime manifold \mathcal{M} foliated by spacelike hypersurfaces Σ_t labeled by time coordinate t . The line element takes the form

$$ds^2 = -N^2 dt^2 + q_{ab}(dx^a + N^a dt)(dx^b + N^b dt), \quad (\text{A1})$$

where:

- $N(t, x^a)$ is the lapse function, measuring proper time between adjacent hypersurfaces
- $N^a(t, x^b)$ is the shift vector, relating spatial coordinates on adjacent hypersurfaces
- $q_{ab}(t, x^c)$ is the spatial metric on Σ_t

The inverse spacetime metric is

$$g^{\mu\nu} = \begin{pmatrix} -N^{-2} & N^{-2}N^a \\ N^{-2}N^b & q^{ab} - N^{-2}N^a N^b \end{pmatrix}. \quad (\text{A2})$$

b. Extrinsic Curvature

The extrinsic curvature K_{ab} of Σ_t embedded in \mathcal{M} is defined as

$$K_{ab} = \frac{1}{2N} (\dot{q}_{ab} - \mathcal{L}_{\vec{N}} q_{ab}) = \frac{1}{2N} (\dot{q}_{ab} - D_a N_b - D_b N_a), \quad (\text{A3})$$

where D_a is the covariant derivative compatible with q_{ab} , and $\mathcal{L}_{\vec{N}}$ denotes Lie derivative along the shift.

The trace is $K = q^{ab} K_{ab}$.

c. ADM Action for General Relativity

Substituting the ADM decomposition into the Einstein-Hilbert action

$$S_{EH} = \frac{1}{16\pi G} \int d^4 x \sqrt{-g} R, \quad (\text{A4})$$

and integrating by parts yields (setting $16\pi G = 1$)

$$S_{ADM} = \int dt \int_{\Sigma} d^3 x N \sqrt{q} \left[{}^{(3)}R + K_{ab} K^{ab} - K^2 \right], \quad (\text{A5})$$

where ${}^{(3)}R$ is the Ricci scalar of the spatial metric q_{ab} .

d. Canonical Variables and Hamiltonian

Define the canonical momentum conjugate to q_{ab} :

$$\pi^{ab} = \frac{\delta L}{\delta \dot{q}_{ab}} = \sqrt{q}(K^{ab} - Kq^{ab}). \quad (\text{A6})$$

The Hamiltonian is

$$H_{ADM} = \int_{\Sigma} d^3x (N\mathcal{C} + N^a\mathcal{C}_a), \quad (\text{A7})$$

where the Hamiltonian and diffeomorphism constraints are

$$\mathcal{C} = G_{abcd}\pi^{ab}\pi^{cd} - \sqrt{q}{}^{(3)}R \approx 0, \quad (\text{A8a})$$

$$\mathcal{C}_a = -2D_b\pi_a^b \approx 0, \quad (\text{A8b})$$

with the DeWitt supermetric

$$G_{abcd} = \frac{1}{2\sqrt{q}}(q_{ac}q_{bd} + q_{ad}q_{bc} - 2q_{ab}q_{cd}). \quad (\text{A9})$$

2. Ashtekar-Barbero Variables

The Ashtekar formulation [51, 67] recasts the gravitational phase space in terms of an $SU(2)$ connection and its conjugate.

a. Densitized Triad and Connection

Introduce a spatial triad $e_a^i(x)$ such that

$$q_{ab} = \delta_{ij}e_a^i e_b^j, \quad (\text{A10})$$

with inverse (co-triad) e_i^a satisfying $e_i^a e_j^j = \delta_i^j$ and $e_i^a e_i^b = \delta_a^b$.

Define the densitized triad:

$$E_i^a = \sqrt{q}e_i^a, \quad \text{with} \quad \det(E_i^a) = \sqrt{q}. \quad (\text{A11})$$

The Ashtekar-Barbero connection is

$$A_a^i = \Gamma_a^i + \gamma K_a^i, \quad (\text{A12})$$

where:

- Γ_a^i is the spin connection compatible with e_a^i :

$$\Gamma_a^i = -\epsilon^{ijk}e_j^b(\partial_a e_{bk} - \partial_b e_{ak}), \quad (\text{A13})$$

- $K_a^i = K_{ab}e^{bi}$ is the extrinsic curvature in triad components
- γ is the Barbero-Immirzi parameter [52, 53]

b. Canonical Structure

The canonical Poisson brackets are

$$\{A_a^i(x), E_j^b(y)\} = 8\pi G\gamma\delta_a^i\delta_j^b\delta^{(3)}(x, y). \quad (\text{A14})$$

c. Hamiltonian in Ashtekar Variables

The gravitational Hamiltonian becomes [68]

$$H_g = \int d^3x (N\mathcal{C}_g + N^a\mathcal{C}_{g,a} + \Lambda^i\mathcal{G}_i), \quad (\text{A15})$$

with constraints

$$\mathcal{C}_g = -\frac{1}{8\pi G\gamma^2} \frac{\epsilon^{ijk}E_i^a E_j^b}{\sqrt{\det E}} [F_{ab}^k - (1 + \gamma^2)\epsilon_{mn}^k K_a^m K_b^n] \approx 0, \quad (\text{A16a})$$

$$\mathcal{C}_{g,a} = F_{ab}^i E_i^b \approx 0, \quad (\text{A16b})$$

$$\mathcal{G}_i = D_a^{(A)} E_i^a = \partial_a E_i^a + \epsilon_{ijk} A_a^j E^{ak} \approx 0, \quad (\text{A16c})$$

where $F_{ab}^i = 2\partial_{[a} A_{b]}^i + \epsilon_{ijk}^i A_a^j A_b^k$ is the curvature of A_a^i .

3. Brans-Dicke Theory in ADM Variables

a. ADM Decomposition of BD Action

The Brans-Dicke action (8) in ADM form becomes

$$\begin{aligned} S_{BD} = \int dt \int_{\Sigma} d^3x N\sqrt{q} & \left[\phi \left({}^{(3)}R + K_{ab}K^{ab} - K^2 \right) \right. \\ & - \frac{\omega}{\phi N^2} \left(\dot{\phi} - N^a \partial_a \phi \right)^2 \\ & + \frac{\omega}{\phi} q^{ab} \partial_a \phi \partial_b \phi \\ & \left. + \frac{2}{N} \left(\dot{\phi} - N^a \partial_a \phi \right) K \right]. \end{aligned} \quad (\text{A17})$$

b. Canonical Variables for Scalar Field

The scalar field has canonical momentum

$$p_{\phi} = \frac{\delta L_{BD}}{\delta \dot{\phi}} = \frac{2\sqrt{q}}{N} \left[K\phi - \frac{\omega}{\phi}(\dot{\phi} - N^a \partial_a \phi) \right], \quad (\text{A18})$$

with Poisson bracket $\{\phi(x), p_{\phi}(y)\} = \delta^{(3)}(x, y)$.

c. BD Hamiltonian Constraint

After Legendre transformation and expressing K_{ab} in terms of momenta, the Hamiltonian constraint becomes (for spatially homogeneous configurations)

$$\mathcal{H}_{BD} = \mathcal{H}_g[\phi] + \mathcal{H}_{\phi}[p_{\phi}, \phi] \approx 0, \quad (\text{A19})$$

where the precise form depends on ω . For $\omega \neq -3/2$, this reduces to Eq. (9) after symmetry reduction to Bianchi I.

4. Bianchi I Symmetry Reduction

a. Diagonal Metric Ansatz

For Bianchi I, the spatial metric is diagonal and homogeneous:

$$q_{ab}dx^a dx^b = a_1^2(t)dx_1^2 + a_2^2(t)dx_2^2 + a_3^2(t)dx_3^2. \quad (\text{A20})$$

Choose a fiducial flat metric \mathring{q}_{ab} with $\mathring{q}_{ab}dx^a dx^b = dx_1^2 + dx_2^2 + dx_3^2$.

b. Fiducial Cell and Volume

Since spacetime is noncompact, integrals over Σ diverge. We introduce a fiducial cell \mathcal{V}_0 with edges L_i and volume $V_0 = L_1 L_2 L_3$. All integrations are restricted to \mathcal{V}_0 .

c. Reduced Canonical Variables

For Bianchi I with fiducial triad $\mathring{e}_i^a = \delta_i^a$, the Ashtekar variables take the form given in Eq. (3):

$$A_a^i = c_i(L_i)^{-1} \mathring{e}_a^i, \quad E_i^a = p_i L_i V_0^{-1} \sqrt{\mathring{q}} \mathring{e}_i^a, \quad (\text{A21})$$

with (c_i, p_i) time-dependent functions satisfying (4).

d. Spin Connection for Bianchi I

For diagonal Bianchi I, the spin connection vanishes: $\Gamma_a^i = 0$. This simplifies the curvature:

$$F_{ab}^i = \gamma \left(2\partial_{[a} K_{b]}^i + \gamma \epsilon_{jk}^i K_a^j K_b^k \right). \quad (\text{A22})$$

In terms of (c_i, p_i) , after imposing homogeneity and integrating over \mathcal{V}_0 , the Hamiltonian constraint reduces to Eq. (9) for $\omega \neq -3/2$ and Eq. (11) for $\omega = -3/2$.

e. Relation to Scale Factors

The scale factors are related to p_i by Eq. (5). These can be derived from

$$a_i = \frac{(\det E)^{1/3}}{|E_i^i|^{1/2}} = \frac{(p_1 p_2 p_3)^{1/6}}{|p_i|^{1/2}}, \quad (\text{A23})$$

with appropriate sign choices for orientation.

Appendix B: Explicit Equations of Motion

We provide the complete equations of motion for the effective quantum systems studied in Secs. IV A and IV B.

1. Effective Poisson Algebra

The quantum moments satisfy a closed Poisson algebra derived from canonical commutation relations [41]. For a single degree of freedom (q, p) :

$$\{\Delta(q^2), \Delta(p^2)\} = 4\Delta(qp), \quad (\text{B1a})$$

$$\{\Delta(q^2), \Delta(qp)\} = 2\Delta(q^2), \quad (\text{B1b})$$

$$\{\Delta(p^2), \Delta(qp)\} = -2\Delta(p^2), \quad (\text{B1c})$$

$$\{q, \Delta(q^2)\} = 2\Delta(qp), \quad (\text{B1d})$$

$$\{p, \Delta(q^2)\} = 0, \quad (\text{B1e})$$

$$\{q, \Delta(p^2)\} = 0, \quad (\text{B1f})$$

$$\{p, \Delta(p^2)\} = -2\Delta(qp), \quad (\text{B1g})$$

$$\{q, \Delta(qp)\} = \Delta(p^2), \quad (\text{B1h})$$

$$\{p, \Delta(qp)\} = -\Delta(q^2). \quad (\text{B1i})$$

For multiple degrees of freedom, additional brackets involve cross-correlations:

$$\{q_i, \Delta(q_j p_k)\} = \delta_{ij} \Delta(p_k^2) + \delta_{ik} \Delta(q_j p_k), \quad (\text{B2a})$$

$$\{p_i, \Delta(q_j p_k)\} = -\delta_{ij} \Delta(q_k^2) - \delta_{ik} \Delta(q_j q_k), \quad (\text{B2b})$$

$$\{\Delta(q_i p_i), \Delta(q_j p_j)\} = \Delta(p_i p_j) \Delta(q_i q_j) - \Delta(q_i p_j) \Delta(p_i q_j) \quad (i \neq j). \quad (\text{B2c})$$

2. Equations for Expectation Values: $\omega \neq -3/2$

The evolution of expectation values is given by $\dot{f} = \{f, H_{\text{eff}}\}$. For our system:

$$\dot{c}_1 = \frac{\partial H_{\text{eff}}}{\partial p_1} = \frac{\partial H_{\text{BD}}}{\partial p_1} + \sum_{a,b} \frac{\partial^2 H_{\text{BD}}}{\partial p_1 \partial x_{ab}} \Delta(x_{ab}), \quad (\text{B3a})$$

$$\dot{c}_2 = \frac{\partial H_{\text{eff}}}{\partial p_2} = \frac{\partial H_{\text{BD}}}{\partial p_2} + \sum_{a,b} \frac{\partial^2 H_{\text{BD}}}{\partial p_2 \partial x_{ab}} \Delta(x_{ab}), \quad (\text{B3b})$$

$$\dot{c}_3 = \frac{\partial H_{\text{eff}}}{\partial p_3} = \frac{\partial H_{\text{BD}}}{\partial p_3} + \sum_{a,b} \frac{\partial^2 H_{\text{BD}}}{\partial p_3 \partial x_{ab}} \Delta(x_{ab}), \quad (\text{B3c})$$

$$\dot{p}_1 = -\frac{\partial H_{\text{eff}}}{\partial c_1} = -\frac{\partial H_{\text{BD}}}{\partial c_1} - \sum_{a,b} \frac{\partial^2 H_{\text{BD}}}{\partial c_1 \partial x_{ab}} \Delta(x_{ab}), \quad (\text{B3d})$$

$$\dot{p}_2 = -\frac{\partial H_{\text{eff}}}{\partial c_2} = -\frac{\partial H_{\text{BD}}}{\partial c_2} - \sum_{a,b} \frac{\partial^2 H_{\text{BD}}}{\partial c_2 \partial x_{ab}} \Delta(x_{ab}), \quad (\text{B3e})$$

$$\dot{p}_3 = -\frac{\partial H_{\text{eff}}}{\partial c_3} = -\frac{\partial H_{\text{BD}}}{\partial c_3} - \sum_{a,b} \frac{\partial^2 H_{\text{BD}}}{\partial c_3 \partial x_{ab}} \Delta(x_{ab}), \quad (\text{B3f})$$

$$\dot{\phi} = \frac{\partial H_{\text{eff}}}{\partial p_{\phi}} = \frac{\partial H_{\text{BD}}}{\partial p_{\phi}} + \sum_{a,b} \frac{\partial^2 H_{\text{BD}}}{\partial p_{\phi} \partial x_{ab}} \Delta(x_{ab}), \quad (\text{B3g})$$

$$\dot{p}_{\phi} = -\frac{\partial H_{\text{eff}}}{\partial \phi} = -\frac{\partial H_{\text{BD}}}{\partial \phi} - \sum_{a,b} \frac{\partial^2 H_{\text{BD}}}{\partial \phi \partial x_{ab}} \Delta(x_{ab}), \quad (\text{B3h})$$

where x_{ab} collectively denotes all phase space variables $(c_i, p_i, \phi, p_{\phi})$, and the sums run over all quantum moments.

Explicitly, from Eq. (14) plus quantum corrections:

$$\begin{aligned}\dot{c}_1 = & \frac{1}{\phi\sqrt{p}} \left[-c_1(c_2p_2 + c_3p_3 - 2\zeta T) + \frac{S - \zeta T^2}{2p_1} \right] \\ & + \frac{1}{\sqrt{p}} \left[\frac{p_1^2\zeta}{\phi} \frac{\partial}{\partial p_1} \Delta(c_1^2) + \frac{2p_1\zeta}{\sqrt{p}} \frac{\partial}{\partial p_1} \Delta(c_1p_\phi) + \dots \right],\end{aligned}\quad (B4)$$

and similarly for other expectation values. The full expressions are lengthy; we implement them numerically using Mathematica.

3. Equations for Quantum Moments: $\omega \neq -3/2$

For quantum dispersions (diagonal moments), the evolution is:

$$\begin{aligned}\frac{1}{2}\dot{\Delta}(c_1^2) = & \frac{\partial^2 H_{\text{eff}}}{\partial p_1^2} \Delta(c_1p_1) + \frac{\partial^2 H_{\text{eff}}}{\partial c_1 \partial p_1} \Delta(c_1^2) \\ & + \sum_{j \neq 1} \left[\frac{\partial^2 H_{\text{eff}}}{\partial p_1 \partial c_j} \Delta(c_1c_j) + \frac{\partial^2 H_{\text{eff}}}{\partial p_1 \partial p_j} \Delta(c_1p_j) \right] \\ & + \frac{\partial^2 H_{\text{eff}}}{\partial p_1 \partial \phi} \Delta(c_1\phi) + \frac{\partial^2 H_{\text{eff}}}{\partial p_1 \partial p_\phi} \Delta(c_1p_\phi),\end{aligned}\quad (B5a)$$

$$\begin{aligned}\frac{1}{2}\dot{\Delta}(p_1^2) = & -\frac{\partial^2 H_{\text{eff}}}{\partial c_1^2} \Delta(c_1p_1) - \frac{\partial^2 H_{\text{eff}}}{\partial c_1 \partial p_1} \Delta(p_1^2) \\ & - \sum_{j \neq 1} \left[\frac{\partial^2 H_{\text{eff}}}{\partial c_1 \partial c_j} \Delta(p_1c_j) + \frac{\partial^2 H_{\text{eff}}}{\partial c_1 \partial p_j} \Delta(p_1p_j) \right] \\ & - \frac{\partial^2 H_{\text{eff}}}{\partial c_1 \partial \phi} \Delta(p_1\phi) - \frac{\partial^2 H_{\text{eff}}}{\partial c_1 \partial p_\phi} \Delta(p_1p_\phi),\end{aligned}\quad (B5b)$$

with analogous equations for $\Delta(c_2^2)$, $\Delta(p_2^2)$, $\Delta(c_3^2)$, $\Delta(p_3^2)$, $\Delta(\phi^2)$, $\Delta(p_\phi^2)$. For covariances (e.g., $\Delta(c_1p_1)$):

$$\begin{aligned}\dot{\Delta}(c_1p_1) = & -\frac{\partial^2 H_{\text{eff}}}{\partial c_1^2} \Delta(c_1^2) + \frac{\partial^2 H_{\text{eff}}}{\partial p_1^2} \Delta(p_1^2) \\ & - \sum_{j \neq 1} \left[\frac{\partial^2 H_{\text{eff}}}{\partial c_1 \partial c_j} \Delta(c_1c_j) + \frac{\partial^2 H_{\text{eff}}}{\partial c_1 \partial p_j} \Delta(c_1p_j) \right] \\ & + \sum_{j \neq 1} \left[\frac{\partial^2 H_{\text{eff}}}{\partial p_1 \partial c_j} \Delta(p_1c_j) + \frac{\partial^2 H_{\text{eff}}}{\partial p_1 \partial p_j} \Delta(p_1p_j) \right] \\ & - \frac{\partial^2 H_{\text{eff}}}{\partial c_1 \partial \phi} \Delta(c_1\phi) + \frac{\partial^2 H_{\text{eff}}}{\partial p_1 \partial \phi} \Delta(p_1\phi) \\ & - \frac{\partial^2 H_{\text{eff}}}{\partial c_1 \partial p_\phi} \Delta(c_1p_\phi) + \frac{\partial^2 H_{\text{eff}}}{\partial p_1 \partial p_\phi} \Delta(p_1p_\phi).\end{aligned}\quad (B6)$$

For cross-correlations (e.g., $\Delta(c_1p_2)$):

$$\begin{aligned}\dot{\Delta}(c_1p_2) = & \frac{\partial^2 H_{\text{eff}}}{\partial p_1^2} \Delta(p_1p_2) - \frac{\partial^2 H_{\text{eff}}}{\partial c_2^2} \Delta(c_1c_2) \\ & + \frac{\partial^2 H_{\text{eff}}}{\partial c_1 \partial p_1} \Delta(c_1p_2) - \frac{\partial^2 H_{\text{eff}}}{\partial c_1 \partial c_2} \Delta(c_1^2) \\ & + \frac{\partial^2 H_{\text{eff}}}{\partial p_1 \partial c_2} [\Delta(c_2p_2) - \Delta(c_1p_1)] + \frac{\partial^2 H_{\text{eff}}}{\partial p_1 \partial p_2} \Delta(p_2^2) \\ & + \sum_{k \neq 1,2} \left[\frac{\partial^2 H_{\text{eff}}}{\partial p_1 \partial c_k} \Delta(p_2c_k) + \frac{\partial^2 H_{\text{eff}}}{\partial p_1 \partial p_k} \Delta(p_2p_k) \right] \\ & - \sum_{k \neq 1,2} \left[\frac{\partial^2 H_{\text{eff}}}{\partial c_2 \partial c_k} \Delta(c_1c_k) + \frac{\partial^2 H_{\text{eff}}}{\partial c_2 \partial p_k} \Delta(c_1p_k) \right] \\ & + \frac{\partial^2 H_{\text{eff}}}{\partial p_1 \partial \phi} \Delta(p_2\phi) - \frac{\partial^2 H_{\text{eff}}}{\partial c_2 \partial \phi} \Delta(c_1\phi) \\ & + \frac{\partial^2 H_{\text{eff}}}{\partial p_1 \partial p_\phi} \Delta(p_2p_\phi) - \frac{\partial^2 H_{\text{eff}}}{\partial c_2 \partial p_\phi} \Delta(c_1p_\phi).\end{aligned}\quad (B7)$$

Similar expressions hold for all 28 cross-correlations. The complete system comprises 48 coupled nonlinear ODEs.

[1] A. Einstein, Relativitats- teorie, *Annale der Physic* **49**, 769 (1916).

[2] A. Einstein, *Sitzungsberichte der Königlich Preußischen Akademie der Wissenschaften* , 688 (1916).

[3] A. Einstein *et al.*, *Annalen der Physik* **35**, 898 (1911).

[4] K. Schwarzschild, *Sitzungsberichte der königlich preussischen Akademie der Wissenschaften* , 189 (1916).

[5] B. P. Abbott, R. Abbott, T. D. Abbott, M. R. Abernathy, F. Acernese, K. Ackley, C. Adams, T. Adams, P. Addesso, R. X. Adhikari, *et al.*, *Physical review letters* **116**, 061102 (2016).

[6] S. W. Hawking and R. Penrose, *Proceedings of the Royal Society of London. A. Mathematical and Physical Sciences* **314**, 529 (1970).

[7] R. Penrose, *Nuovo Cimento Rivista Serie* **1**, 252 (1969).

[8] V. C. Rubin, W. K. Ford Jr, and N. Thonnard, *Astrophysical Journal, Part 1*, vol. 238, June 1, 1980, p. 471-487. **238**, 471 (1980).

[9] T. M. Abbott, F. B. Abdalla, A. Alarcon, J. Aleksić, S. Allam, S. Allen, A. Amara, J. Annis, J. Asorey, S. Avila, *et al.*, *Physical Review D* **98**, 043526 (2018).

[10] A. G. Riess, A. V. Filippenko, P. Challis, A. Clocchiatti, A. Diercks, P. M. Garnavich, R. L. Gilliland, C. J. Hogan, S. Jha, R. P. Kirshner, *et al.*, *The astronomical journal* **116**, 1009 (1998).

[11] S. Perlmutter, G. Aldering, G. Goldhaber, R. A. Knop, P. Nugent, P. G. Castro, S. Deustua, S. Fabbro, A. Goobar, D. E. Groom, *et al.*, *The Astrophysical Journal* **517**, 565 (1999).

[12] C. Brans and R. H. Dicke, *Physical review* **124**, 925 (1961).

[13] C. M. Will, *Living reviews in relativity* **17**, 1 (2014).

[14] A. Avilez and C. Skordis, *Physical review letters* **113**, 011101 (2014).

[15] V. Faraoni, in *Cosmology in Scalar-Tensor Gravity* (Springer, 2004) pp. 1–53.

[16] C. R. Almeida, O. Galkina, and J. C. Fabris, *Universe* **7**, 286 (2021).

[17] A. Batista, J. Fabris, and R. de Sa Ribeiro, *General Relativity and Gravitation* **33**, 1237 (2001).

[18] J. P. de Leon, *Classical and Quantum Gravity* **27**, 095002 (2010).

[19] Ö. Delice, *Physical Review D—Particles, Fields, Gravitation, and Cosmology* **74**, 124001 (2006).

[20] O. Hrycyna, M. Szydłowski, and M. Kamionka, *arXiv preprint arXiv:1404.7112* (2014).

[21] A. H. Ziae and M. R. Mehdizadeh, *Classical and Quantum Gravity* **41**, 145001 (2024).

[22] C.-Y. Lin, X. Liu, Y. Ma, and C. Zhang, *Physical Review D* **108**, 124074 (2023).

[23] G. J. Olmo and H. Sanchis-Alepuz, *Physical Review D—Particles, Fields, Gravitation, and Cosmology* **83**, 104036 (2011).

[24] T. P. Sotiriou and V. Faraoni, *Reviews of Modern Physics* **82**, 451 (2010).

[25] Y. Bisabr, *arXiv e-prints* , arXiv (2024).

[26] Y. Bisabr, *arXiv preprint arXiv:2403.13303* (2024).

[27] E. Di Valentino, O. Mena, S. Pan, L. Visinelli, W. Yang, A. Melchiorri, D. F. Mota, A. G. Riess, and J. Silk, *Classical and Quantum Gravity* **38**, 153001 (2021).

[28] M. A. Troxel, N. MacCannan, J. Zuntz, T. Ei- fler, E. Krause, S. Dodelson, D. Gruen, J. Blazek, O. Friedrich, S. Samuroff, *et al.*, *Physical Review D* **98**, 043528 (2018).

[29] Y. Aditya, D. Tejeswararao, and U. D. Prasanthi, *East European Journal of Physics* , 85 (2024).

[30] Pinki, P. Kumar, and C. Singh, *Modern Physics Letters A* **39**, 2450046 (2024).

[31] C. Rovelli, *Quantum gravity* (Cambridge university press, 2004).

[32] A. Ashtekar and P. Singh, *Classical and Quantum Gravity* **28**, 213001 (2011).

[33] M. Bojowald, *Physical Review Letters* **86**, 5227 (2001).

[34] A. Ashtekar, T. Pawłowski, and P. Singh, *Physical review letters* **96**, 141301 (2006).

[35] E. M. Lifshitz and I. M. Khalatnikov, *Advances in Physics* **12**, 185 (1963).

[36] V. A. Belinski, I. M. Khalatnikov, and E. M. Lifshitz, *Advances in Physics* **19**, 525 (1970).

[37] I. Agullo, A. Ashtekar, and W. Nelson, *Physical Review D—Particles, Fields, Gravitation, and Cosmology* **87**, 043507 (2013).

[38] A. Ashtekar and E. Wilson-Ewing, *Physical Review D—Particles, Fields, Gravitation, and Cosmology* **79**, 083535 (2009).

[39] E. Wilson-Ewing, *Physical Review D—Particles, Fields, Gravitation, and Cosmology* **82**, 043508 (2010).

[40] M. Bojowald and A. Skirzewski, *Reviews in Mathematical Physics* **18**, 713 (2006).

[41] M. Bojowald, *Classical and Quantum Gravity* **29**, 213001 (2012).

[42] M. Bojowald, *Physical Review D—Particles, Fields, Gravitation, and Cosmology* **75**, 081301 (2007).

[43] M. Bojowald, H. Hernández, and A. Skirzewski, *Physical Review D—Particles, Fields, Gravitation, and Cosmology* **76**, 063511 (2007).

[44] H. Hernandez-Hernandez and G. Sanchez-Herrera, *Physical Review D* **110**, 043506 (2024).

[45] L. C. Gomar, M. Martín-Benito, and G. A. M. Marugán, *Journal of Cosmology and Astroparticle Physics* **2015** (06), 045.

[46] M. Bojowald, *Universe* **6**, 125 (2020).

[47] G. Chacón-Acosta, H. Hernández-Hernández, and J. Ruvalcaba-Rascón, *Annals of Physics* **467**, 169695 (2024).

[48] L. Aragón-Muñoz, G. Chacón-Acosta, and H. Hernandez-Hernandez, *International Journal of Modern Physics B* **34**, 2050271 (2020).

[49] M. Bojowald and D. Ding, *Journal of Cosmology and Astroparticle Physics* **2021** (03), 083.

[50] H. H. Hernandez and C. R. J. Valdez, *Physica Scripta* **98**, 025215 (2023).

[51] A. Ashtekar, *Physical review letters* **57**, 2244 (1986).

[52] J. F. Barbero, *arXiv preprint gr-qc/9410014* (1994).

[53] G. Immirzi, *Classical and Quantum Gravity* **14**, L177 (1997).

[54] X. Zhang and Y. Ma, in *Journal of Physics: Conference Series*, Vol. 360 (IOP Publishing, 2012) p. 012055.

[55] M. Sharma, G. S. Vicente, L. L. Graef, R. O. Ramos, and A. Wang, *Physical Review D* **111**, 043501 (2025).

[56] V. Oikonomou, *Nuclear Physics B* **984**, 115985 (2022).

[57] D.-W. Chiou, *Physical Review D—Particles, Fields,*

Gravitation, and Cosmology **75**, 024029 (2007).

[58] X. Zhang and Y. Ma, Physical Review D—Particles, Fields, Gravitation, and Cosmology **84**, 104045 (2011).

[59] F. B. Martínez and J. Olmedo, Physical Review D **93**, 124008 (2016).

[60] S. A. Hayward, Physical review letters **96**, 031103 (2006).

[61] G. J. Olmo, International Journal of Modern Physics D **20**, 413 (2011).

[62] D. B. Blaschke and M. P. Dabrowski, Entropy **14**, 1978 (2012).

[63] R. R. Caldwell, Physics Letters B **545**, 23 (2002).

[64] I. Bars, S.-H. Chen, P. J. Steinhardt, and N. Turok, Physics Letters B **715**, 278 (2012).

[65] E. Elizalde, S. Nojiri, and S. D. Odintsov, Physical Review D **70**, 043539 (2004).

[66] R. L. Arnowitt, S. Deser, and C. W. Misner, Gen. Rel. Grav. **40**, 1997 (2008).

[67] A. Ashtekar, Physical Review D **36**, 1587 (1987).

[68] T. Thiemann, *Modern canonical quantum general relativity* (Cambridge University Press, 2008).